

Supporting Information

Vapochromic Properties of Diethenylpyrrole with Naphthyl Tethers Induced by Formation of a Distorted Structure in the Solid State

Soichi Yokoyama,^{1,2,*} Haruyasu Asahara,^{1,2,3} Nagatoshi Nishiwaki^{1,2,*}

- ¹ School of Environmental Science and Engineering, Kochi University of Technology, Kami, Kochi 782-8502, Japan
² Research Center for Material Science and Engineering, Kochi University of Technology, Kami, Kochi 782-8502, Japan
³ Graduate School of Pharmaceutical Sciences, Osaka University, Yamadaoka 1-6, Suita, Osaka 565-0871, Japan

Supporting Data

Contents	Page
Experimental section	S2-S3
Figure S1	Equipment drawing
Figure S2	Estimated rotation barrier by DFT calculation
Figure S3	UV-vis./FL spectra in various solvent
Table S1	Photophysical properties in various solvent
Figure S4	Simulated absorption spectra and oscillator strength
Table S2	X-ray crystallographic data of single crystal α , β and γ
Figure S5	X-ray structure of single crystal γ .
Table S3	X-ray crystallographic data of single crystal 2 \rightarrow 2,5-DHP
Figure S6	UV-vis./FL spectra in solution and in single crystal α , β and γ
Table S4	Photophysical properties in DCM solution and each single crystals
Figure S7	Change of single crystal α upon exposure to THF vapor
Figure S8	Quantum yield change upon exposure powder of 2 to THF/toluene vapor
Figure S9	Tg chart of pristine powder and 2 \rightarrow THF powder
Figure S10	¹ H NMR chart after exposing of pristine powder to THF vapor
Figure S11	Change of ground powder 1 upon exposure to THF vapor
Figure S12	Fluorescence spectra after exposing pristine powder to various solvent vapor
Figure S13–S21	¹ H NMR chart after exposing pristine powder to various solvent vapor
Figure S22	¹ H NMR chart after exposing 2 \rightarrow THF powder to toluene vapor
Figure S23	Fluorescence spectra after exposing 2 \rightarrow THF powder to various solvent vapor
Figure S24	Thermal stability of 2 \rightarrow THF powder
Figure S25	Stability of 2 \rightarrow THF powder under reduced pressure
Figure S26	Effect of grinding on fluorescence spectra of 2 \rightarrow THF powder
Figure S27	¹ H NMR chart after grinding 2 \rightarrow THF powder
Figure S28	PXRD pattern change of pristine powder 2 upon the exposure to THF vapor
Figure S29	Simulated PXRD pattern of crystal α , β and γ
Figure S30	A plausible mechanism of vapochromism
Table S5 and Figures S31–S34	Fluorescence lifetime analysis
Table S6–S8	Transition states
Figure S35–S36	¹ H, ¹³ C{ ¹ H} NMR data of compound 2
	Cartesian coordination of optimized structures
	References

General.

Unless specifically mentioned, reagents and solvents were obtained from commercial suppliers and used without further purification. All reactions were monitored by thin-layer chromatography carried out on Merck silica gel plates (60F-254). Column chromatography was performed on silica gel (Nacalai Tesque, 70–230 mesh for normal phase). The ^1H NMR and $^{13}\text{C}\{^1\text{H}\}$ NMR spectra were recorded on a Bruker Ascend-400 at 298 K. ^1H and $^{13}\text{C}\{^1\text{H}\}$ chemical shifts are reported in ppm downfield from tetramethylsilane (TMS). High-resolution mass spectra were measured on an AB SCIEX Triple TOFTM 4600 by positive mode. IR spectra were recorded on a JASCO FT/IR-4200 spectrometer equipped with an ATR detector.

Synthesis of 2,5-bis[1-cyano-2-(naphthalen-1-yl)vinyl]-1*H*-pyrrole (**2**)

To a solution of 2,5-bis(cyanomethyl)pyrrole¹ (40.0 mg, 0.275 mmol) and 1-naphthaldehyde (0.132 g, 0.845 mmol) in ethanol (5 mL) was added aqueous solution of benzyltrimethylammonium hydroxide (10 w%, 5 mL). After stirring at 60 °C for 2 hour under Ar, the reaction was quenched by addition of saturated NH_4Cl aqueous solution. The resulting mixture was extracted with dichloromethane. Then, the organic phase was dried over MgSO_4 , filtered and evaporated in vacuo. The crude product was purified by silica column chromatography (DCM/hexane =2/1 to 5/1 as an eluent). Further purification was performed by recrystallization from toluene to afford **2** as a red crystal (80.1 mg, 0.190 mmol, 69%). Mp 213.6–214.8 °C. ^1H NMR (400 MHz, CDCl_3) δ (ppm) 9.02 (bs, 1H), 8.08-7.93 (m, 6H), 7.92-7.90 (m, 4H), 7.59-7.51 (m, 6H), 6.80 (d, 2H, $J = 2.8$ Hz). $^{13}\text{C}\{^1\text{H}\}$ NMR (100 MHz, CDCl_3) δ (ppm) 134.9 (CH), 133.6 (C), 131.5 (CH) 130.9 (C), 130.6 (C), 129.8 (C), 129.0 (CH), 127.1 (CH), 126.9 (CH), 126.5 (CH), 125.5 (CH), 123.3 (CH), 116.7 (C), 111.7 (CH), 105.9 (C). IR (ATR/ cm^{-1}) 3293, 2220, 1586, 1507, 1419, 1286, 1233, 1053. HRMS (ESI-QTOF) m/z $[\text{M} - \text{H}]^-$ calcd for $\text{C}_{30}\text{H}_{18}\text{N}_3$ 420.1506, found 420.1498.

UV–vis. and Fluorescent Spectroscopy.

Absorption spectra were recorded on a JASCO V-650 spectrophotometer. Fluorescence spectra were recorded on a Hamamatsu Quantaurus-QY Plus UV–NIR absolute PL quantum yield spectrometer C13334 or JASCO FP-8300. Quartz cell with 10 mm. Fluorescence quantum yields were determined on a Hamamatsu Quantaurus-QY Plus UV–NIR absolute PL quantum yield spectrometer C13534. Excitation was carried out at 400 nm. Fluorescence decay profiles were recorded on a Hamamatsu Photonics picosecond fluorescence lifetime measurement system C11200 equipped with picosecond light pulsar PLP-10, spectrograph C11119-01, and streak scope C10627, or a Hamamatsu Photonics streak scope C4334 equipped with a spectrograph C5094. Excitation was carried out by a laser diode whose wavelength was $\lambda_{\text{ex}} = 378$ nm (pulse width is around 45 ps) or 441 nm (pulse width is around 76 ps).

X-ray Single Crystal diffraction.

Data collection for X-ray crystal analysis was performed on Rigaku/XtaLAB Synergy-S/Cu or Mo ($\text{CuK}\alpha$ $\lambda = 1.54187$ Å or $\text{MoK}\alpha$ $\lambda = 0.71073$ Å) diffractometers. The single crystal α , β and γ was obtained slow vapor diffusion from chlorobenzene/pentane, THF/hexane and THF/pentane, respectively. The X-ray measurement was performed at -150 °C or -180 °C. The structures were solved by direct methods (SHELXT) and refined through full-matrix least-squares techniques on F^2 using SHELXL and OLEX2 crystallographic software packages.²⁻⁴ All non-hydrogen atoms

were refined with anisotropic displacement parameters and hydrogen atoms were placed at calculated positions and refined “riding” on their corresponding carbon atoms. Crystallographic data are available from Supporting Information or The Cambridge Crystallographic Data Centre, codes 1962397, 1962398, 1962399 and 1962426.

Powder X-ray diffraction

PXRD data were collected on a AERIS (PANalytical) using Ni filter monochromatized Cu-K α radiation (1.54056 Å) with a temperature control unit. XRD patterns ranged from 3° to 30° was repeatedly recorded with a scan rate of 0.14 °/min.

DFT calculation.

The geometrical optimization was carried out for at the B3LYP/6-31+g(d,p) level on Gaussian 09 package.⁵ Convergence at a local minimum structure was confirmed by no imaginary frequencies on frequency analysis. The optimized local minimum structures at the ground states (S_0) were subjected to TD-DFT calculations in the gas phase to obtain 10 excited states from the lowest energy states (S_1). GaussSum 3.0 software was used for the calculation of the minor and major energy contributions of HOMO and LUMO levels for each transition state.⁶

Sample procedure and experiment for exposure to organic solvent vapor

A pristine powder was prepared by grinding the single crystal α over 3 min. Exposure of the sample to organic solvent vapor was performed in Petri dish (Figure. S1). The powder were placed on a glass plate so as not to contact with solvent. The content was covered by a larger Petri dish to diffuse the solvent vapor.

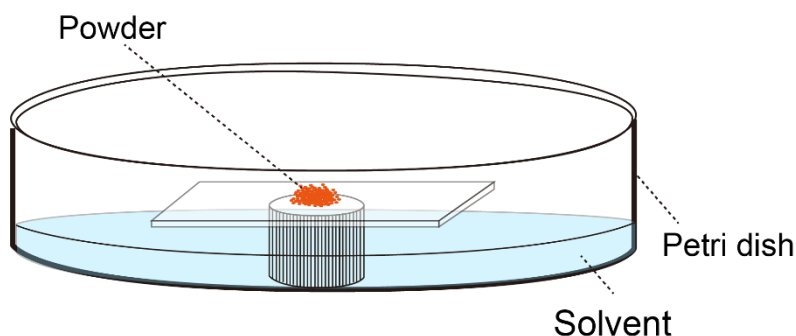


Figure S1 Illustration of experimental method and equipment for the exposure of the sample to organic solvent.

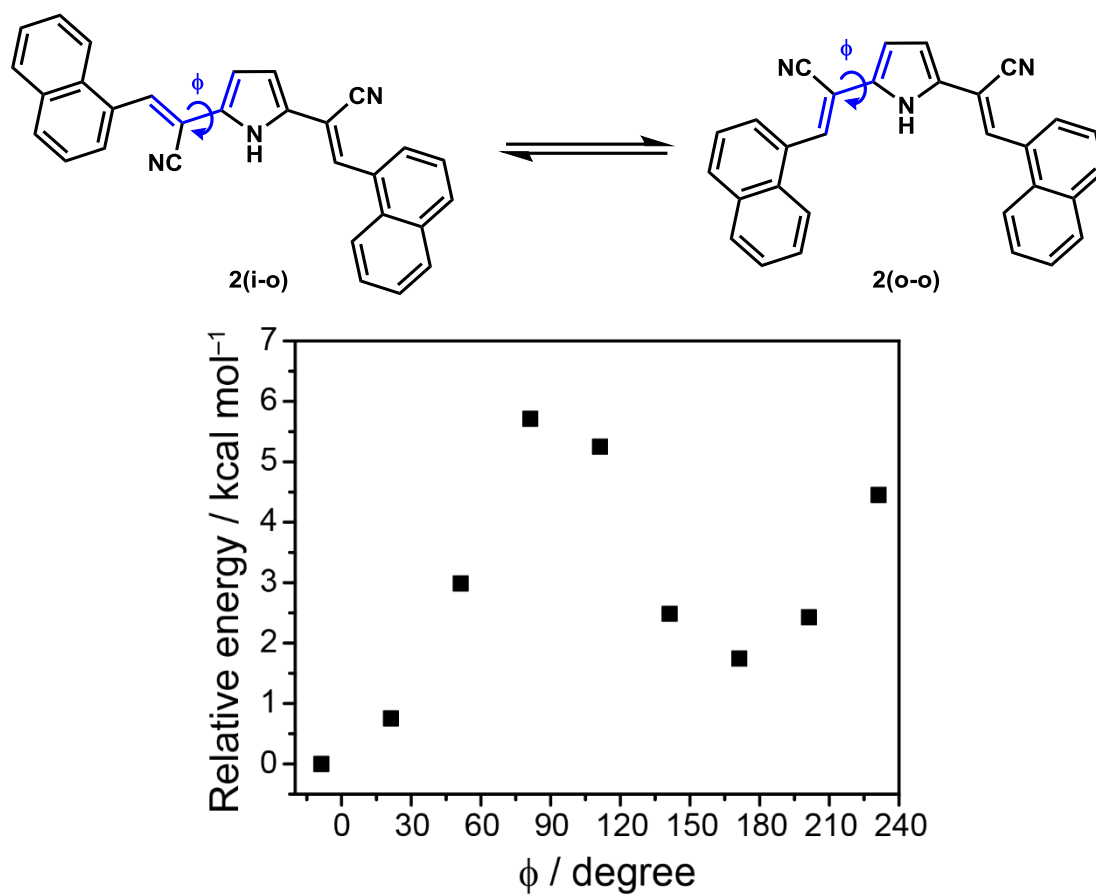


Figure S2 Estimated rotation barrier of a single bond around a pyrrole ring between **2(i-o)** and **2(o-o)**. The relative energy was calculated by B3LYP/6-31g+(d,p) level.

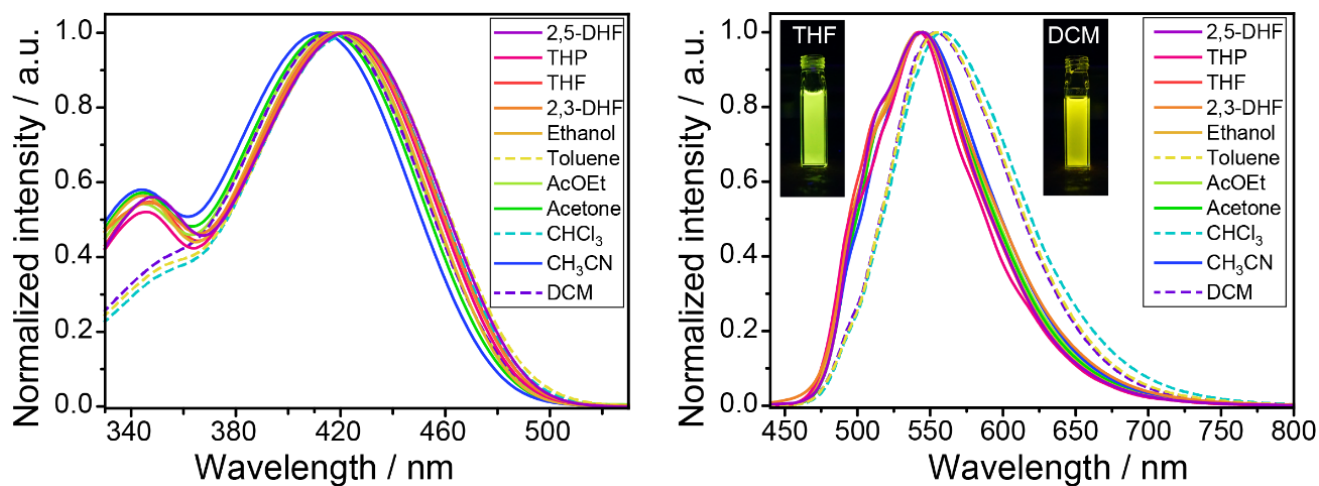


Figure S3 (left) UV-vis. absorption and (right) fluorescence spectra (λ_{ex} = 420 nm) in various solvent.

Table S1. The maximum absorption/fluorescence wavelength and Stokes shift in various solvent.

	λ _{abs} / nm	λ _{fl} / nm	(λ _{fl} - λ _{abs}) / nm	Stokes shift / cm ⁻¹
2,5-DHF	423	545	122	5290
THP	420	542	122	5360
THF	421	544	123	5370
2,3-DHF	421	545	124	5400
Ethanol	419	543	124	5450
Toluene	423	555	132	5620
AcOEt	417	545	128	5630
Acetone	415	545	130	5750
CHCl ₃	421	559	138	5860
CH ₃ CN	412	545	133	5920
DCM	417	554	137	5930

Consideration from the result of TD-DFT calculation

We carried out TD-DFT calculation at B3LYP/6-31g+(d,p) level for each conformer and **2** \supset THF complex. Conformer **2(i-o)** has a smaller oscillator strengths for $S_0 \rightarrow S_3$ transition than those of **2(o-o)** and **2** \supset THF complex (Figure S5). On the other hand, the oscillator strength of **2** at $S_0 \rightarrow S_1$ transition was lowered by interconversion from **2(i-o)** to **2(o-o)** conformer. Focusing on the result of UV-vis. absorption spectra, the absorption band of the compound **2** around 340 nm would be attributed to absorption of $S_0 \rightarrow S_3$ transition. The absorbance in toluene, dichloromethane and chloroform (solvent A: dotted lines in Figure S4a) was relatively lower than that in the other solvent (solvent B: solid line in Figure S4a) that can form hydrogen bonding with a proton donor. Therefore, it is suggested that the conformer **2(o-o)** formed a complex structure in solvent B, resulting in a decreasing concentration of **2(o-i)** and **2(o-o)** with lower oscillator strength in $S_0 \rightarrow S_3$.

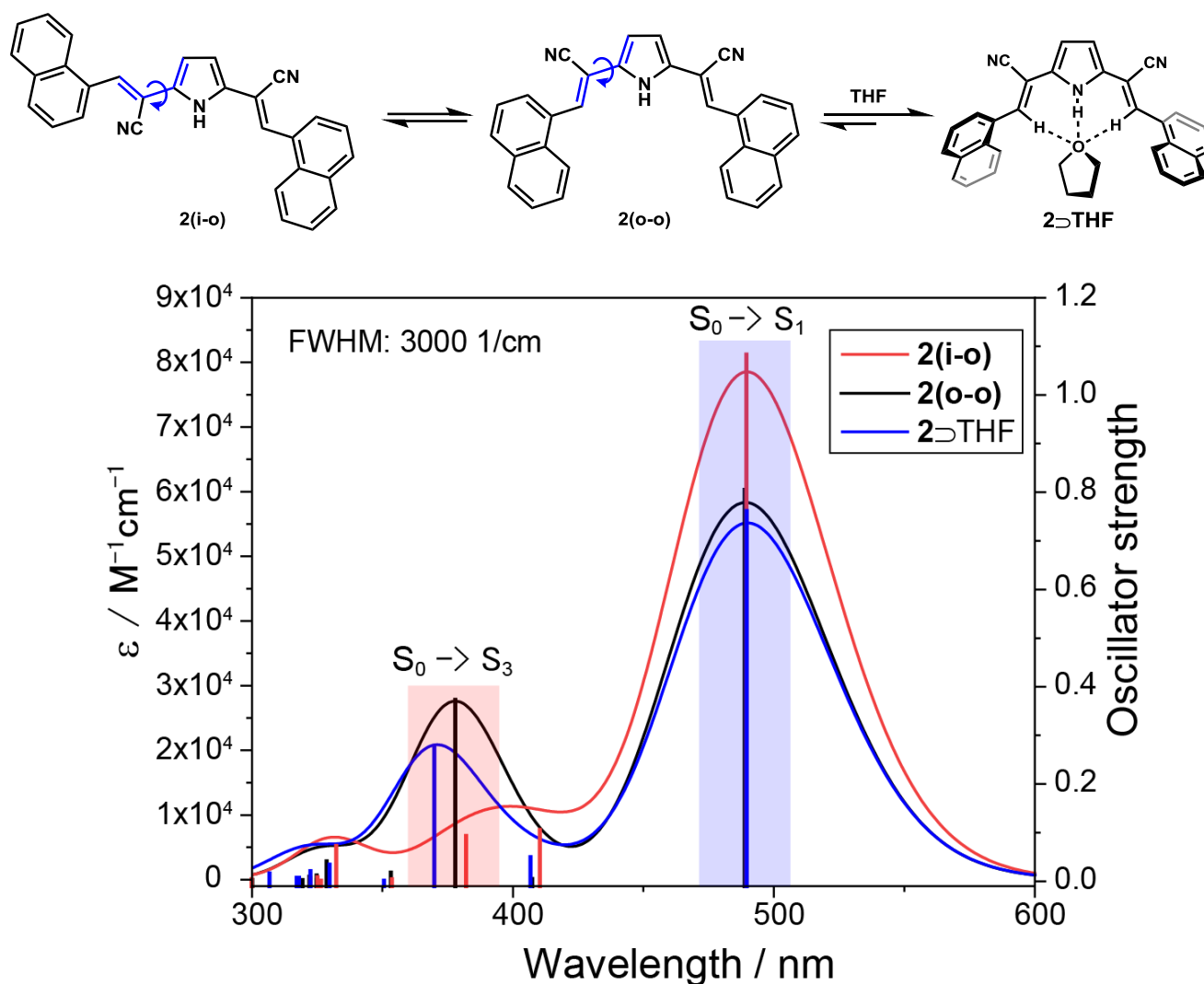
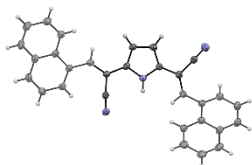
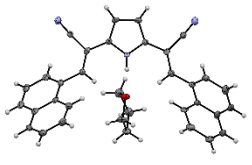
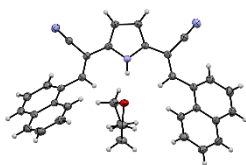


Figure S4 Simulated absorption spectra and oscillator strength for **2(i-o)**, **2(o-o)** and **2** \supset THF at TD-B3LYP/6-31g+(d,p) level. GaussSum 3.0 software was used to simulate the absorption spectra.⁶

Table S2. X-ray crystallographic data of single crystal α , β and γ . ^a

	Crystal α	Crystal β	Crystal γ
Crystal structure			
Chemical formula	C ₃₀ H ₁₅ N ₃	C ₆₈ H ₅₄ N ₃ O	C ₃₄ H ₂₇ N ₃ O
Formula weight	421.48	493.58	493.58
Crystallization Solvent	Chlorobenzene/pentane	THF/pentane	THF/hexane
T / K	93.15 / K	93.15 / K	123 / K
Wavelength / Å	0.71073 (Mo K α)	0.71073 (Mo K α)	1.54184 (Cu K α)
Color	Clear red	Clear yellow	Clear yellow
Crystal size / mm	0.35 \times 0.186 \times 0.08	0.5 \times 0.255 \times 0.042	0.144 \times 0.082 \times 0.043
Crystal system	Monoclinic	Monoclinic	orthorhombic
Space group	P2 ₁ /n	Cc	Pbca
<i>a</i> / Å	7.8509(2)	28.2977(8)	14.8614 (2)
<i>b</i> / Å	12.5211(3)	14.8839(3)	12.58960 (10)
<i>c</i> / Å	21.5915 (5)	12.6181(3)	27.6856 (4)
α / °	90	90	90
β / °	90.115 (2)	102.764(3)	90
γ / °	90	90	90
<i>V</i> / Å ³	2122.48 (9)	5183.2(2)	5179.95 (11)
<i>Z</i>	4	4	8
Density (calculated)	1.313	1.265	1.266
Goodness-of-fit on F ²	1.039	1.045	1.031
<i>R</i> ₁ [<i>I</i> > 2 σ (<i>I</i>)]	0.0350	0.0297	0.0371
w <i>R</i> ₂ (for all data)	0.0886	0.0744	0.0979

^a. The thermal ellipsoids are represented at 50% probability level.

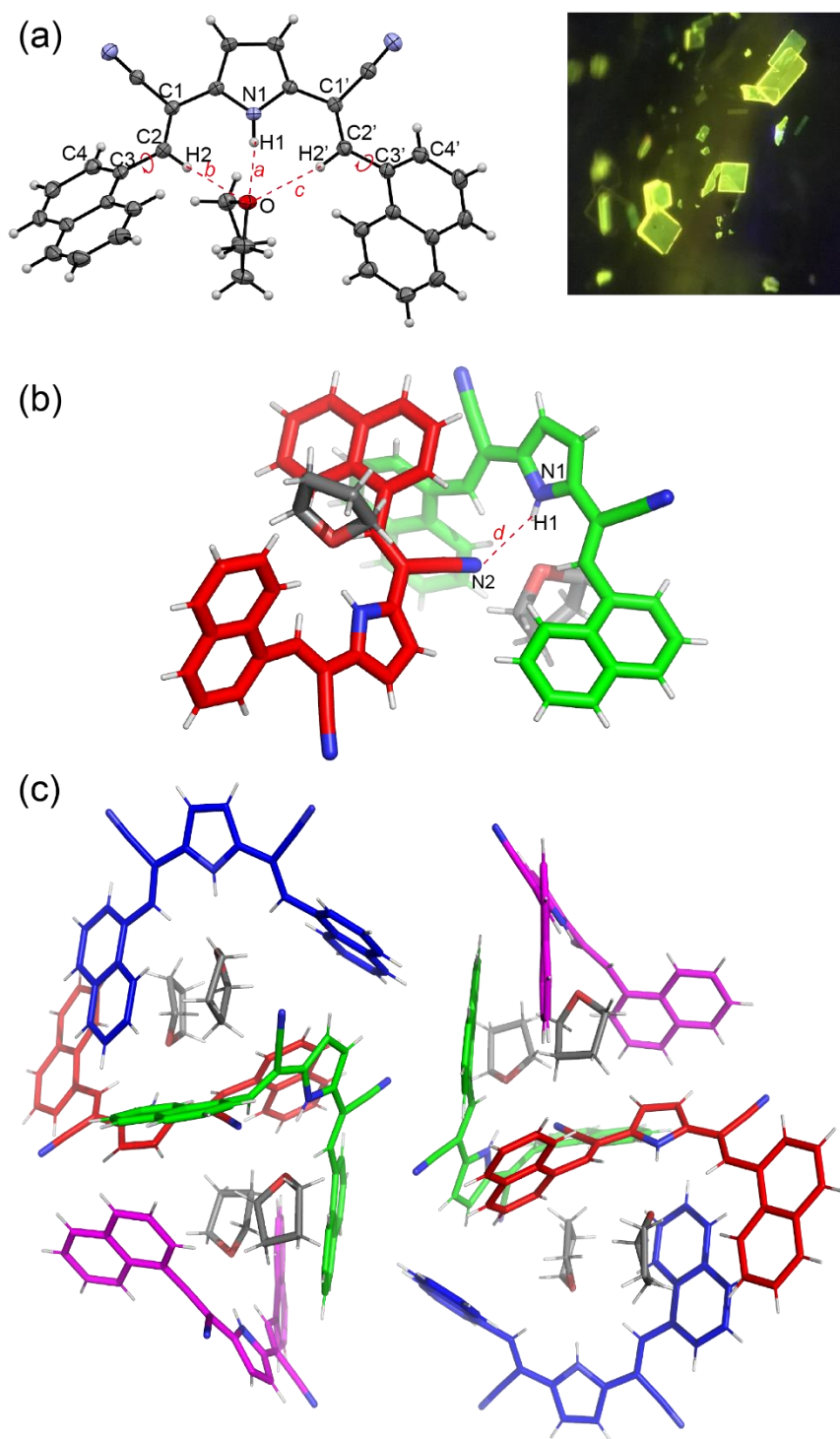
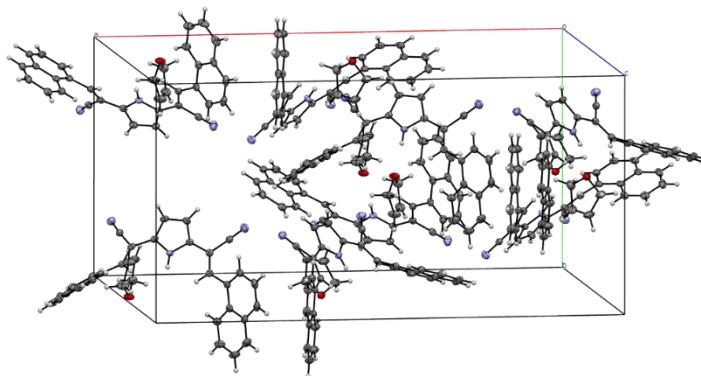
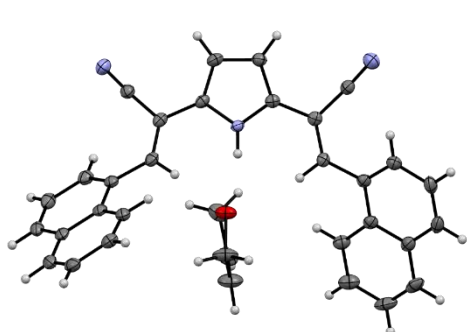


Figure S5 X-ray structure of single crystal γ . (a) A complex structure of **2** with THF. (b) Dimer structure. (c) Packing structure at one unit cell. Red dotted lines denote hydrogen bonding a (N1...O1 = 2.855 Å, N1H1...O = 2.065 Å), b (C2...O = 3.244 Å, C2H2...O1 = 2.615 Å), c (C2'...O = 3.519 Å, N2'H2'...O = 2.621 Å), d (N1...N2 = 3.530 Å, N1H1...N2 = 2.668 Å). Torsional angle around single bond between naphthyl and vinyl group became 43.6 ° for C1–C2–C3–C4 and 34.8 ° for C1'–C2'–C3'–C4'. The thermal ellipsoids are represented at 50% probability level.

Table S3. X-ray crystallographic data of single crystal **2** \supset 2,5-DHP



The thermal ellipsoids are represented at 50% probability level.

Empirical formula	C ₆₈ H ₅₀ N ₆ O ₂
Formula weight	983.14
Temperature/K	93.15
Crystal system	monoclinic
Space group	Cc
a/Å	28.3008(7)
b/Å	14.7916(3)
c/Å	12.7047(4)
α /°	90
β /°	102.621(3)
γ /°	90
Volume/Å ³	5189.9(2)
Z	4
$\rho_{\text{calc}}/\text{cm}^3$	1.258
Crystal size/mm ³	0.862 \times 0.157 \times 0.088
Radiation	MoK α (λ = 0.71073)
Goodness-of-fit on F ²	1.046
Final R indexes [$I \geq 2\sigma(I)$]	R ₁ = 0.0313, wR ₂ = 0.0751
Final R indexes [all data]	R ₁ = 0.0347, wR ₂ = 0.0772

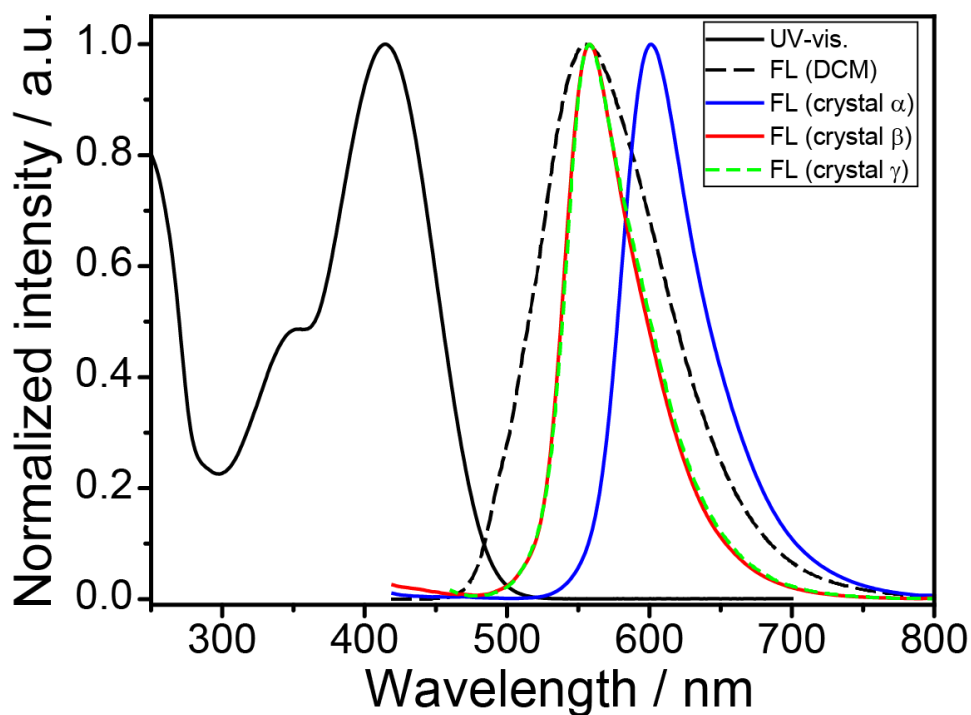


Figure S6 UV-vis. absorption and fluorescence spectra in DCM solution and in single crystal α , β and γ .

Table S4. Photophysical properties in DCM solution and each single crystals.

	λ_{fl} / nm	Φ_f	$\langle \tau_f \rangle$ / ns	k_f / ns ⁻¹	k_{nr} / ns ⁻¹
Solution (DCM)	555	0.08	1.72	0.079	0.91
Crystal α (w/o THF)	601	0.12	2.06	0.058	0.43
Crystal β (2 \supset THF)	558	0.38	3.72	0.10	0.17
Crystal γ (2 \supset THF)	558	0.31	3.41	0.091	0.20

The fluorescence rate constant (k_f) and non-radiative decay rate constant (k_{nr}) were calculated from the fluorescence quantum yield (Φ_f) and the lifetime ($\langle \tau_f \rangle$) using the following equations:⁷

$$\Phi_f = \frac{k_f}{k_f + k_{nr}} = k_f \langle \tau_f \rangle \quad (1)$$

$$\langle \tau_f \rangle^{-1} = k_f + k_{nr} \quad (2)$$

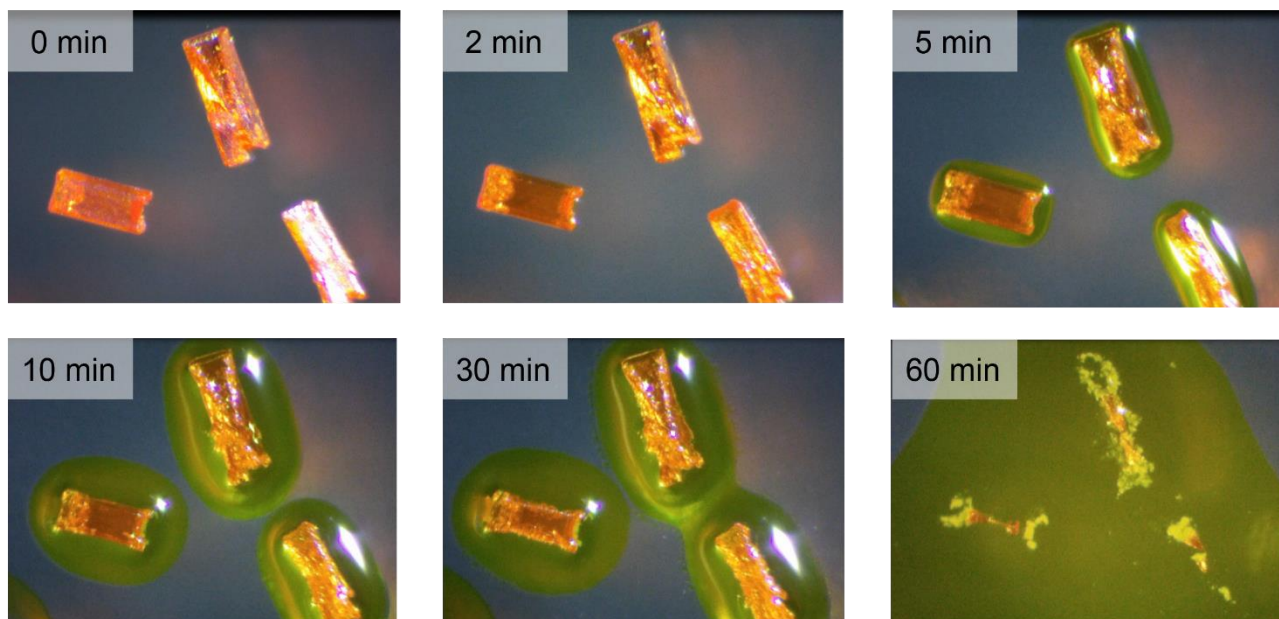
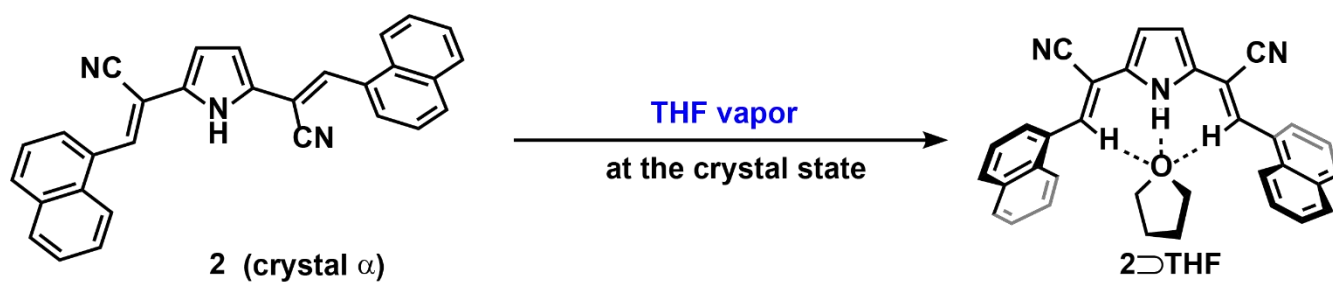


Figure S7 Change of single crystal α upon exposure to THF vapor.

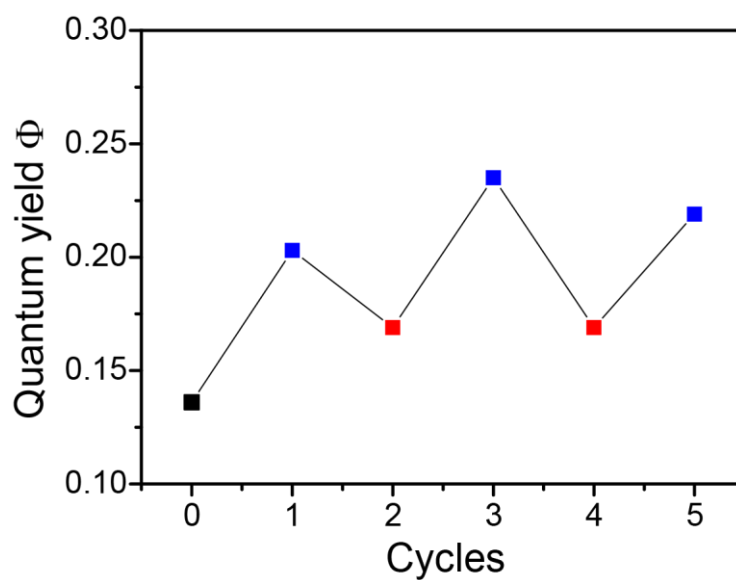


Figure S8 Quantum yield change upon exposure of pristine powder of **2** to THF/toluene. Black square symbol denotes the quantum yield of the pristine powder **2**. Blue and red square symbol denote the quantum yield of powder after exposing to THF or toluene vapor, respectively.

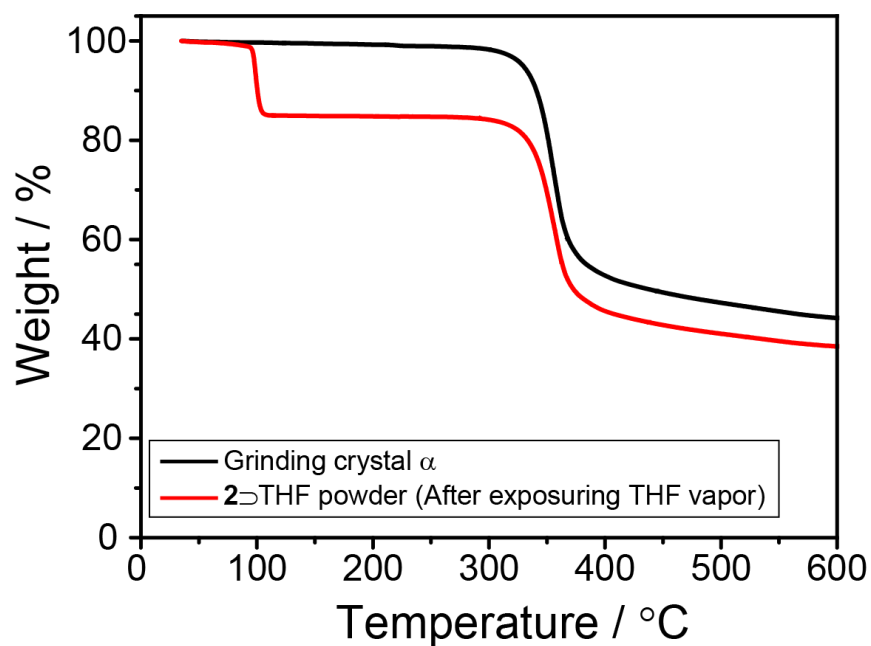


Figure S9 Tg chart of pristine powder (black line) and **2**⊃THF powder (red line). The scan rate was 5 °C/min under N₂ gas flow (100 mL/min)

Estimation of the molar amount of absorbed THF molecules from the result of Tg measurement

Weight of **2**⊃THF powder at 30 °C: 4.315 mg

Weight of the powder after heating at 120 °C: 3.666 mg

The amount of the released THF molecule and the remaining compound **2** becomes 0.649 mg (9.0 μmol) and 3.666 mg (8.7 μmol), respectively. Therefore, the molar ratio of **2**/THF becomes *ca.* 1/1 in the **2**⊃THF powder.

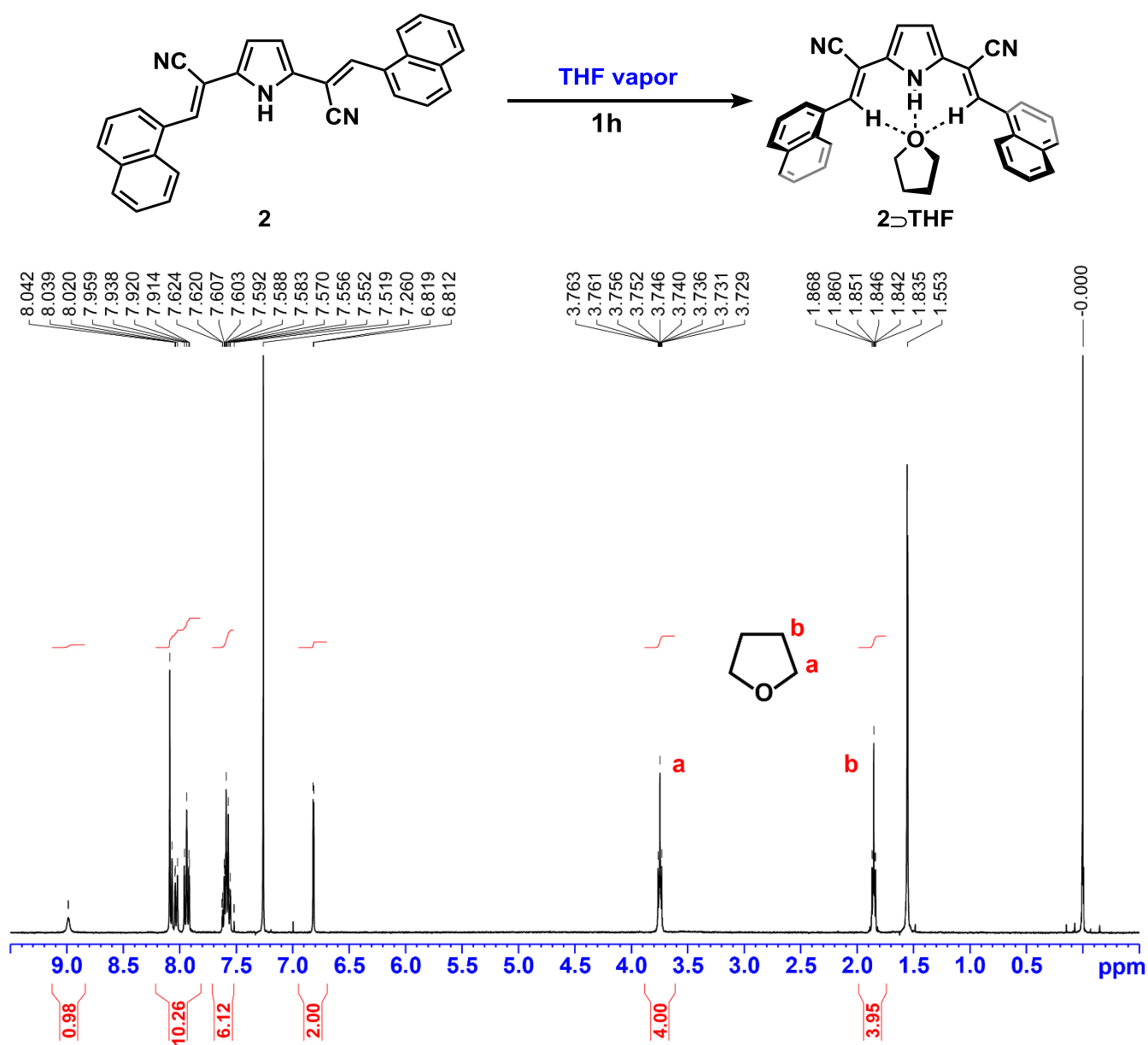


Figure S10. ¹H-NMR (400 MHz, CDCl₃) of **2**⊃THF powder after exposing the pristine powder to THF vapor for 1h. The molar ratio of **2**/THF becomes 1/1.

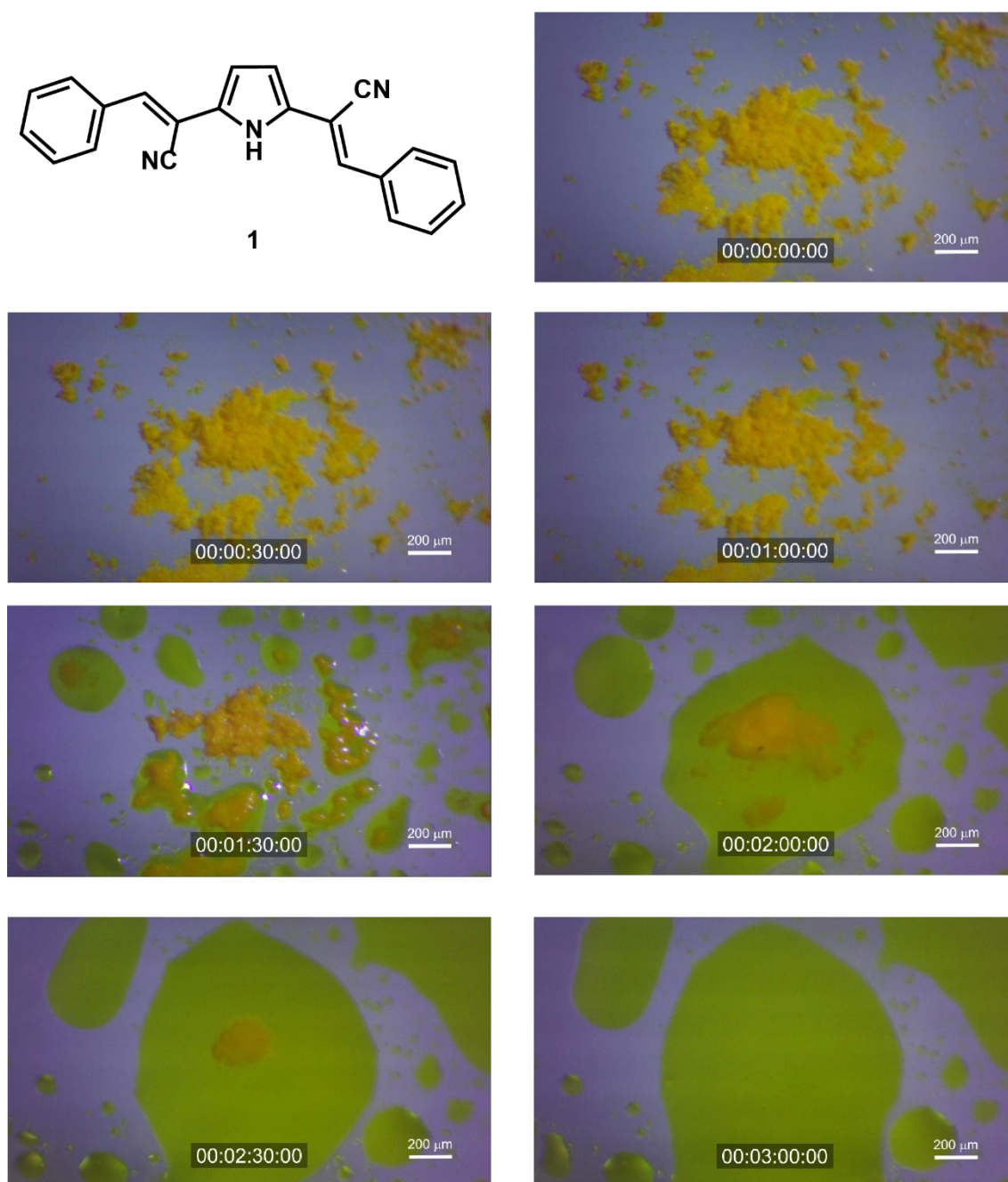
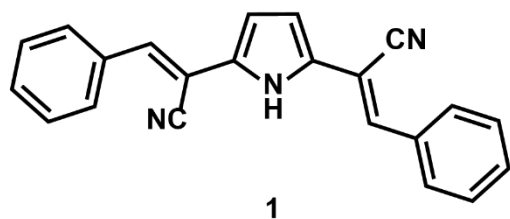


Figure S11 Change of ground powder **1** upon exposure to THF vapor. Timecode was represented at the bottom of each photograph. The display (00:00:00:00) denotes (h:min:sec:10msec).

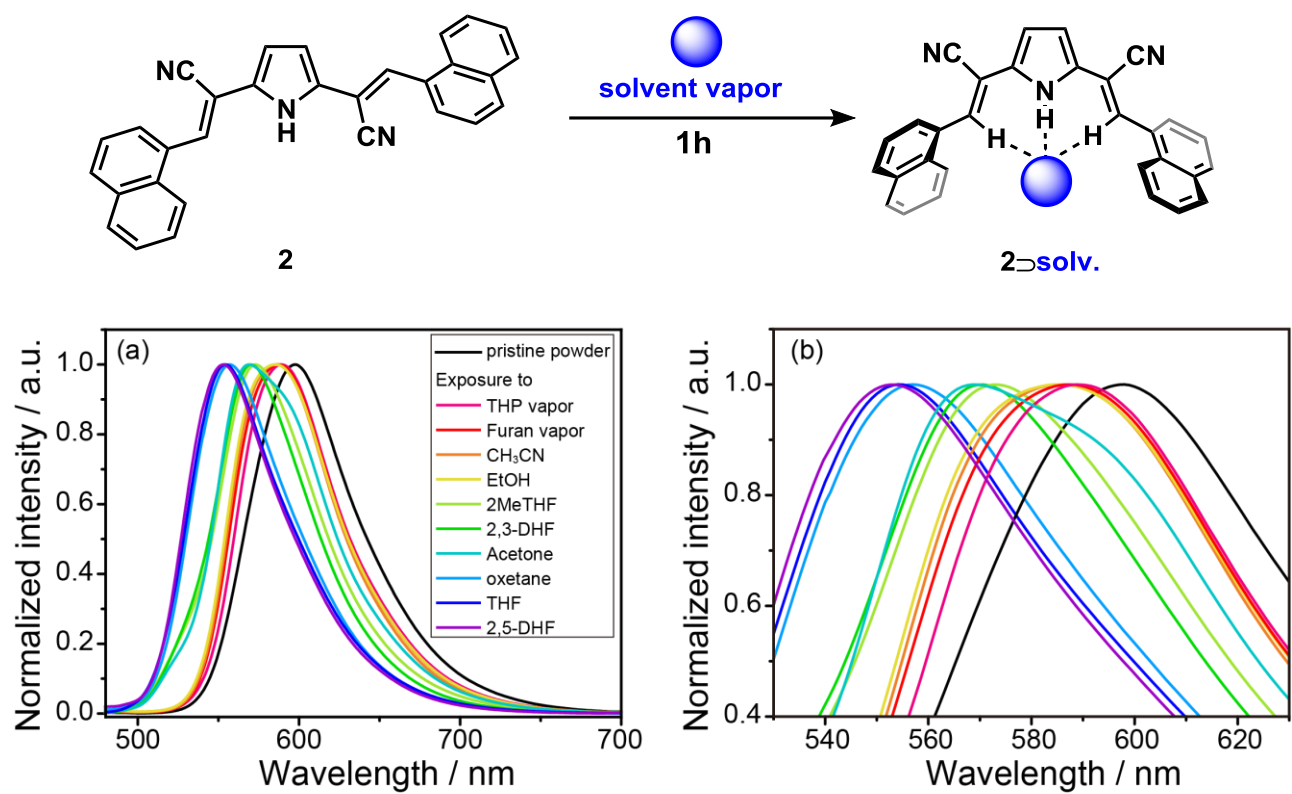


Figure S12 (a) Fluorescence spectra after exposing pristine powder to various solvent vapor for one hour. $\lambda_{\text{ex}} = 400$ nm. (b) An enlarged graph of (a).

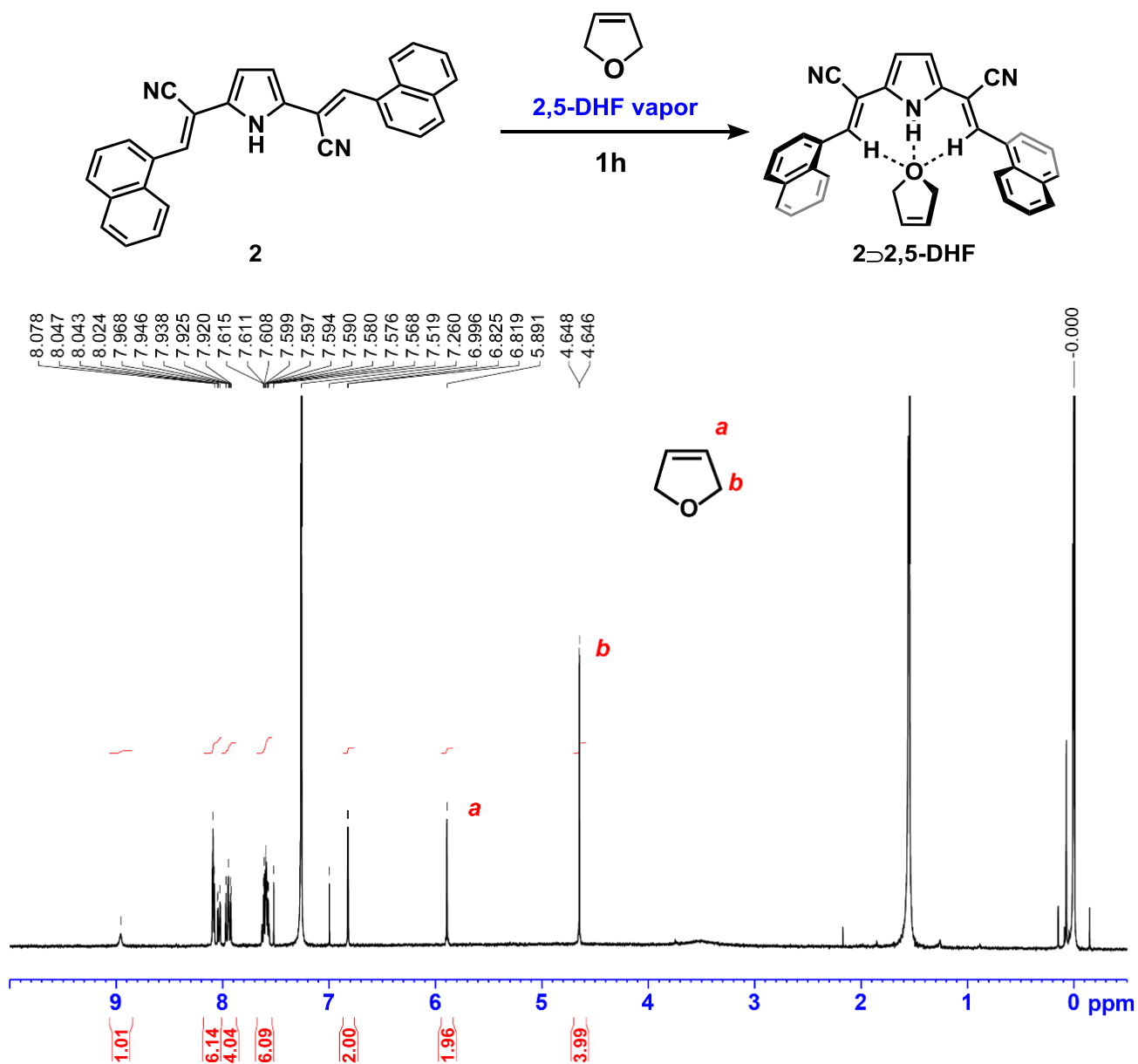


Figure S13. ¹H-NMR (400 MHz, CDCl₃) after exposing the pristine powder to 2,5-dihydrofuran (2,5-DHF) vapor. The exposure of the pristine powder to 2,5-dihydrofuran for 1h. The molar ratio of **2**/THF becomes 1/1.

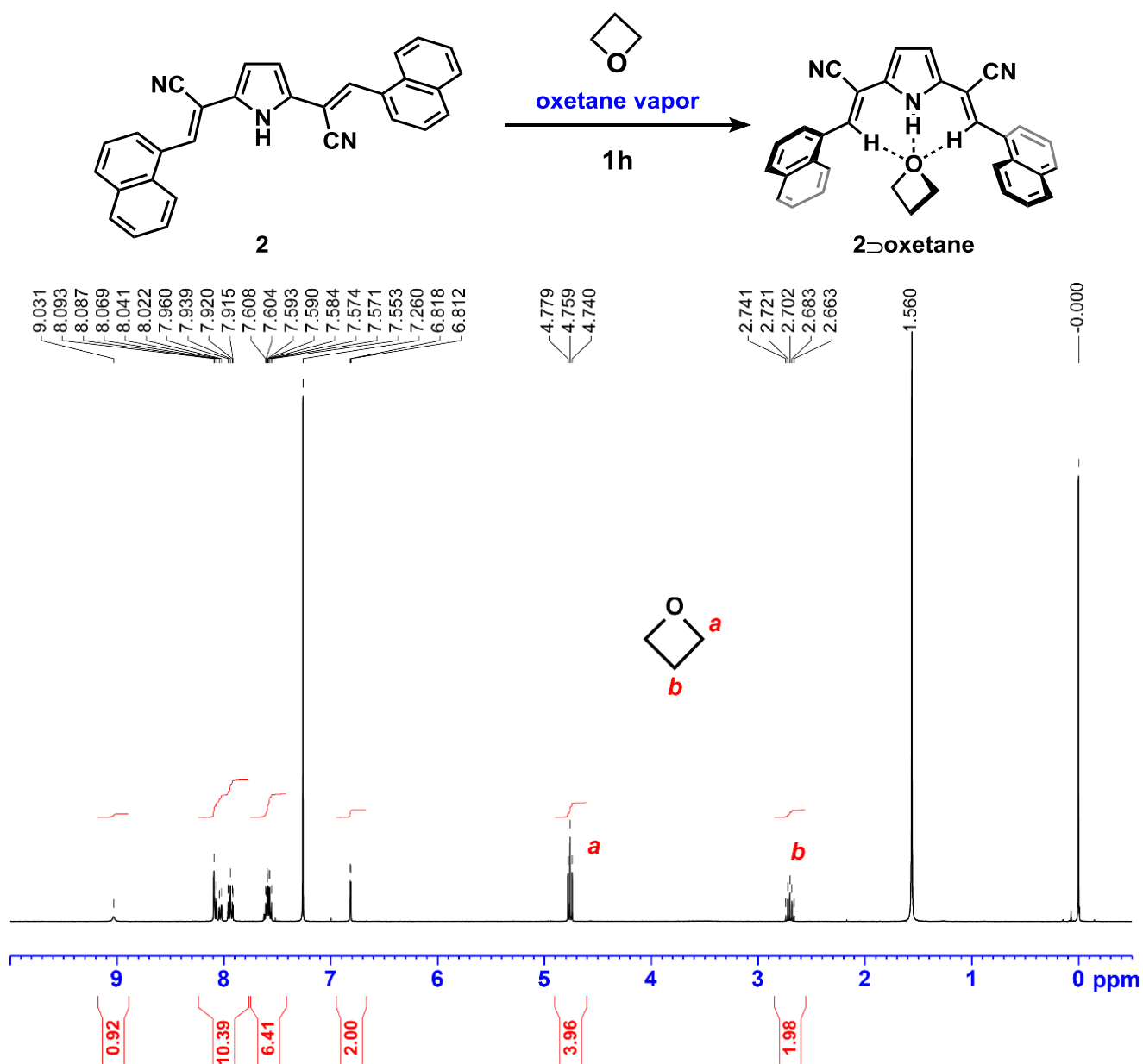


Figure S14 ¹H-NMR (400 MHz, CDCl₃) after exposing the pristine powder to oxetane vapor for 1h. The molar ratio of **2**/oxetane becomes 1/1.

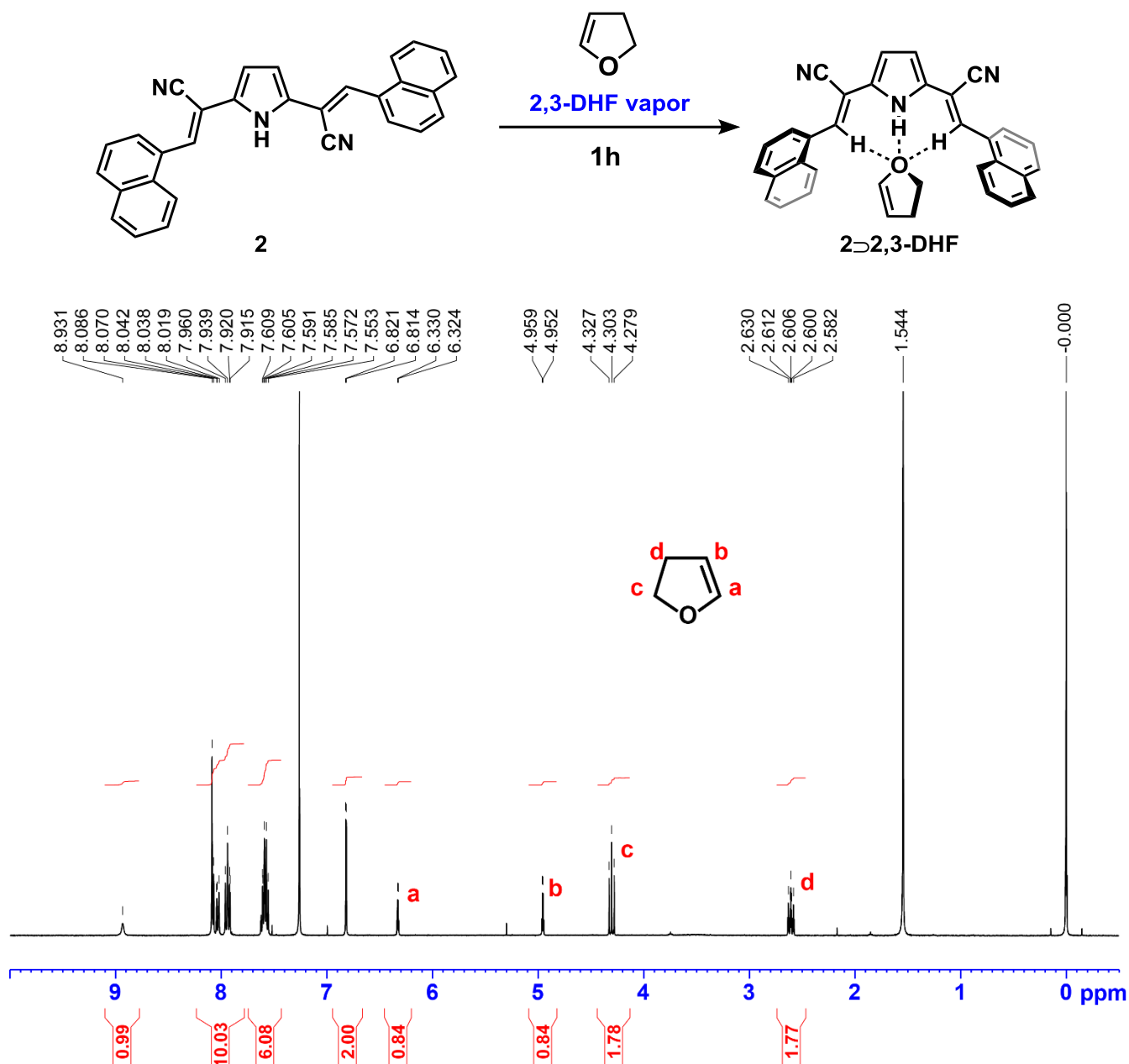


Figure S15 $^1\text{H-NMR}$ (400 MHz, CDCl_3) after exposing the pristine powder to 2,3-dihydrofuran (2,3-DHF) vapor for 1h. The molar ratio of **2**/2,3-DHF becomes 10/9.

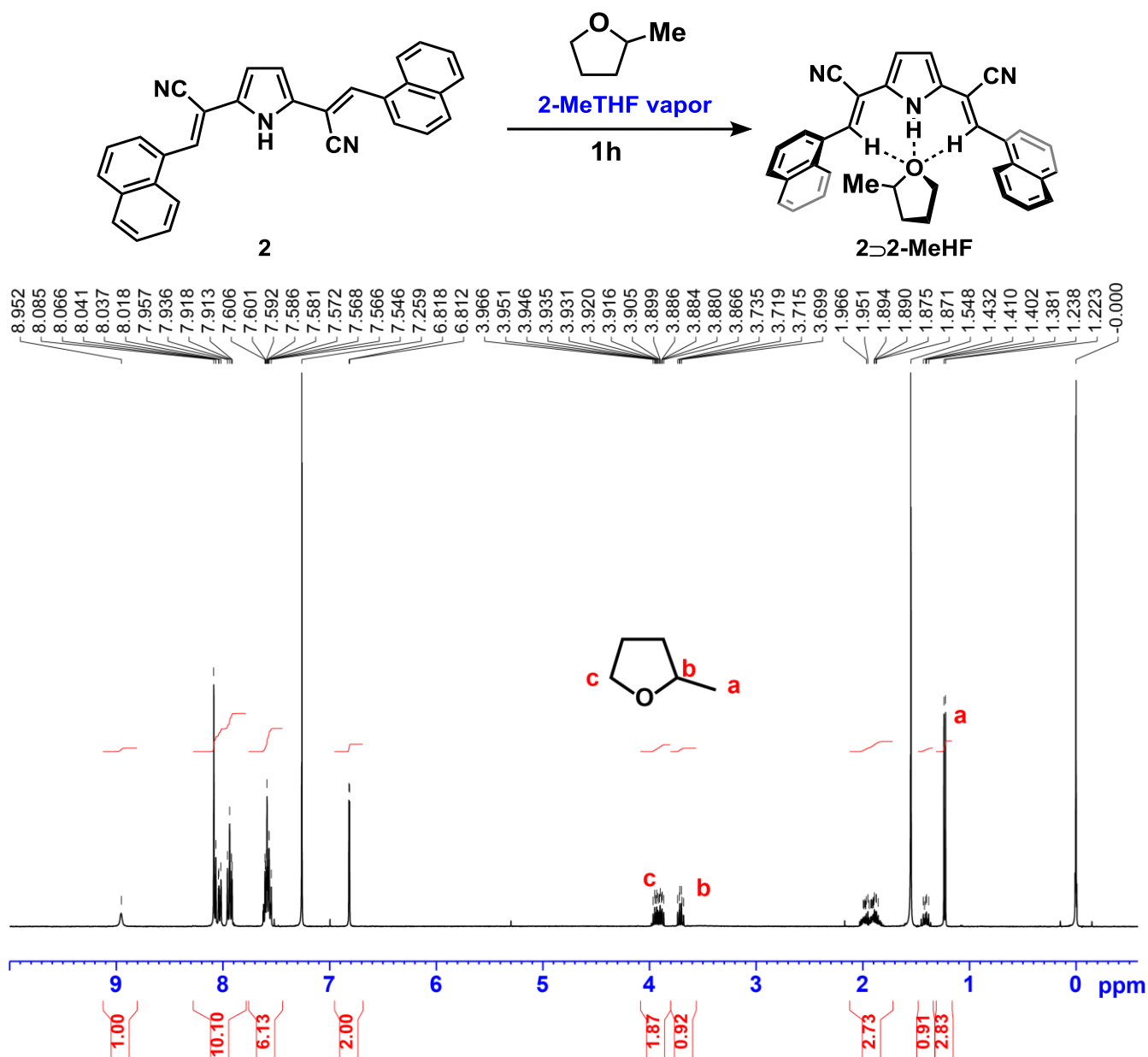


Figure S16 ¹H-NMR (400 MHz, CDCl₃) after exposing the pristine powder to 2-methyltetrahydrofuran (2-MeTHF) vapor for 1h. The molar ratio of **2**/2-MeTHF becomes 10/9.

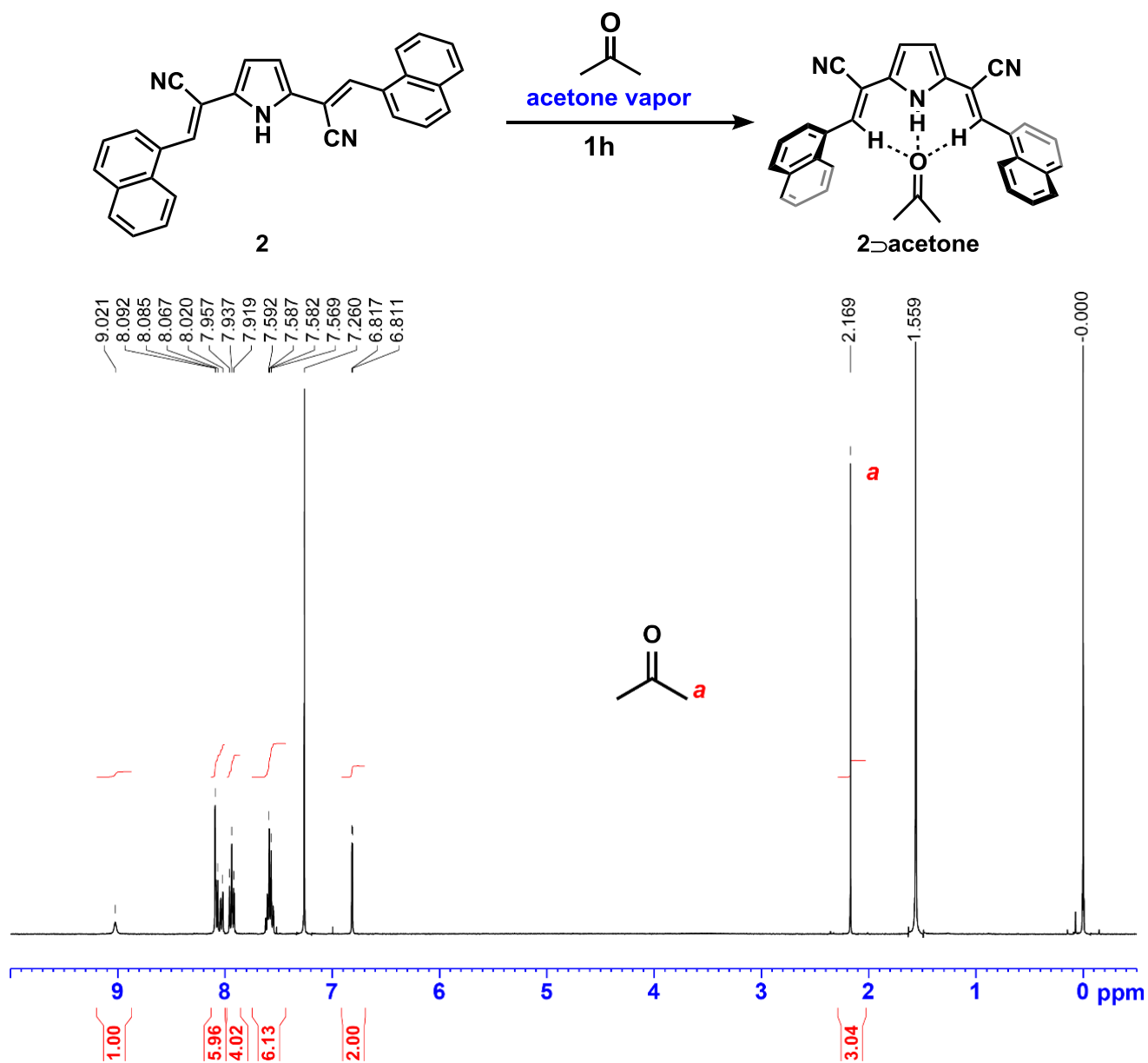


Figure S17 $^1\text{H-NMR}$ (400 MHz, CDCl_3) $^1\text{H-NMR}$ (400 MHz, CDCl_3) after exposing the pristine powder to acetone vapor for 1h. The molar ratio of **2**/acetone becomes 2/1.

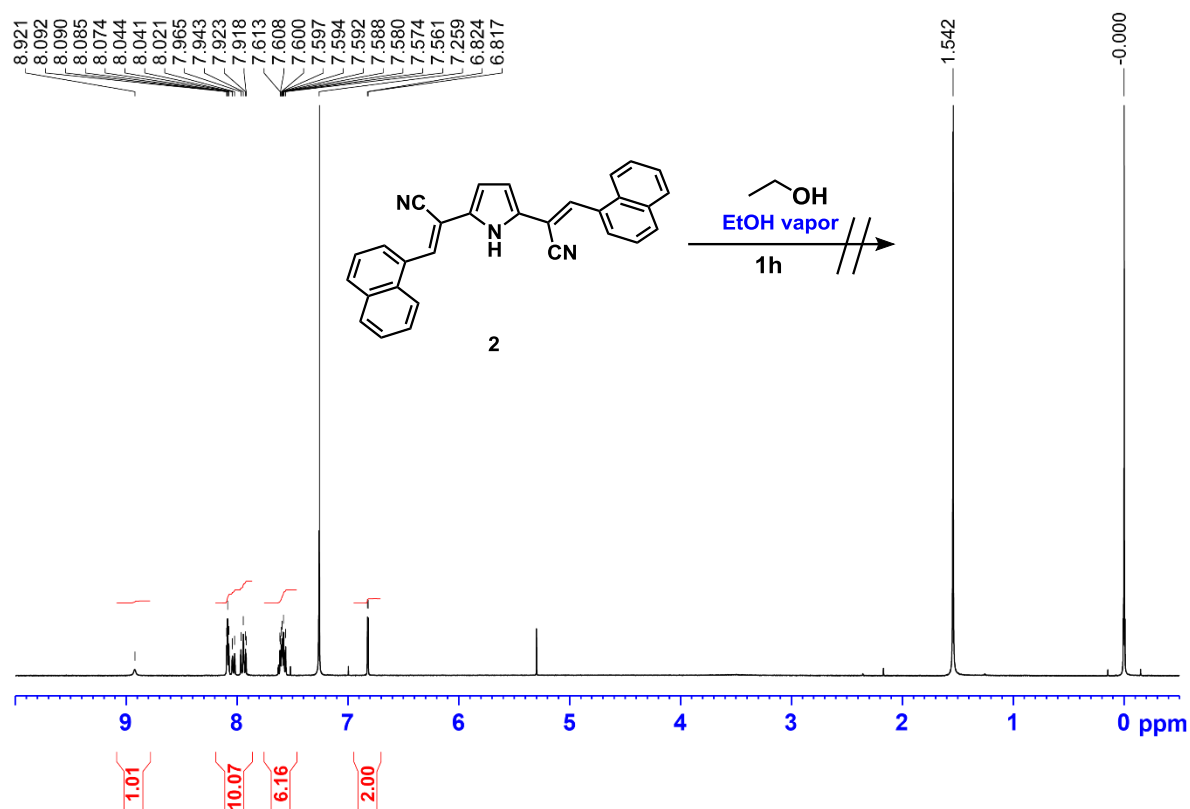


Figure S18 ¹H-NMR (400 MHz, CDCl₃) after exposing the pristine powder to ethanol vapor for 1h. Peaks of ethanol were not observed after the exposure.

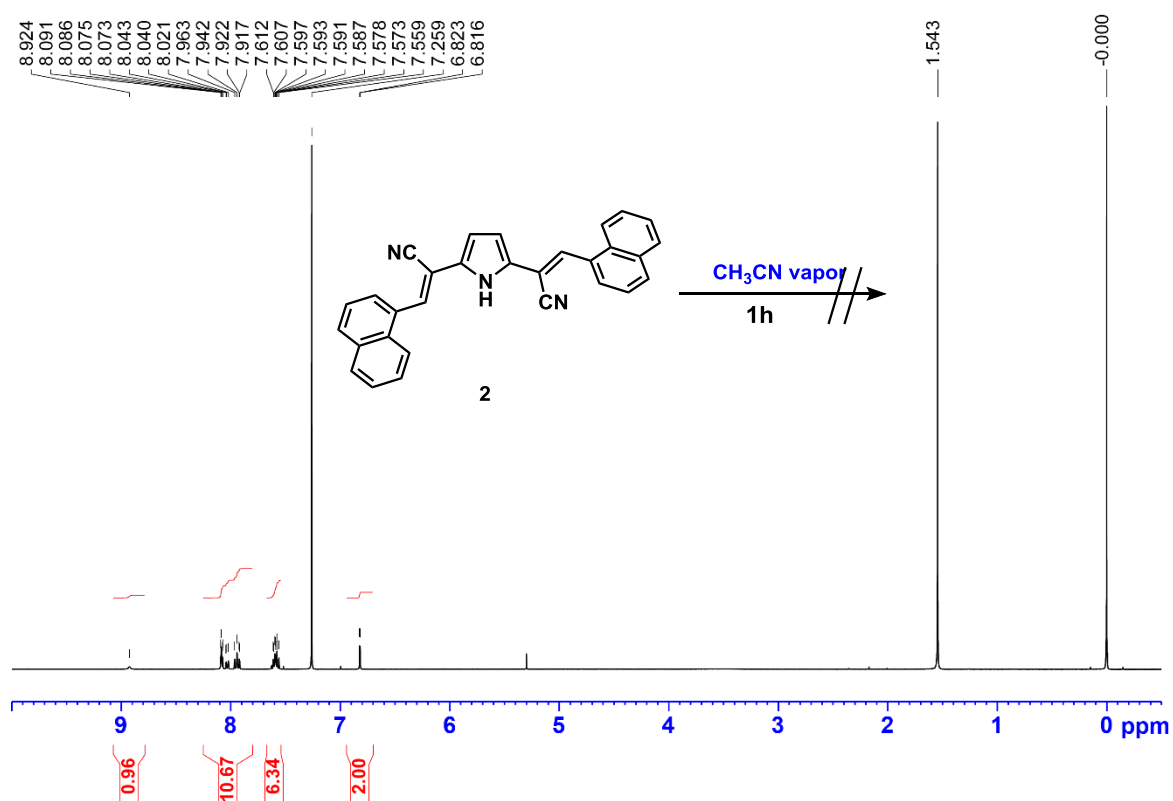


Figure S19 ¹H-NMR (400 MHz, CDCl₃) after exposing the pristine powder to CH₃CN vapor for 1h. Peaks of CH₃CN were not observed after the exposure.

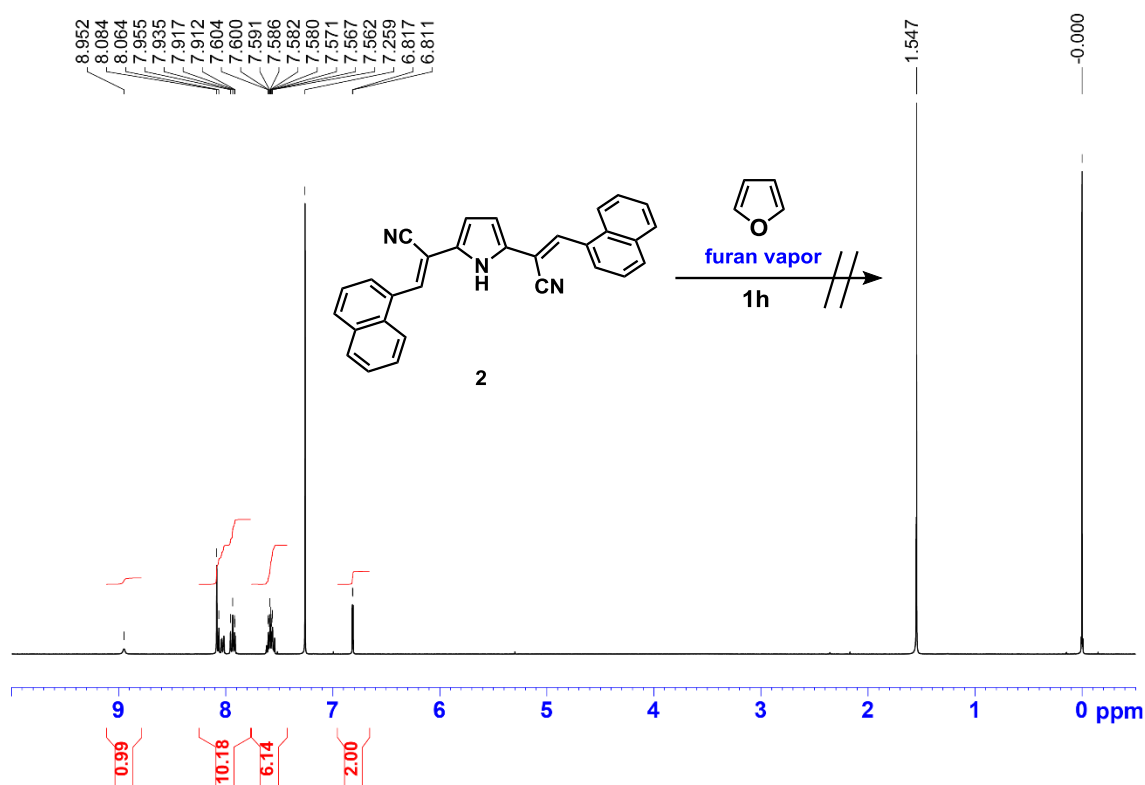


Figure S20 ¹H-NMR (400 MHz, CDCl₃) after exposing the pristine powder to furan vapor for 1h. Peaks of furan were not observed after the exposure.

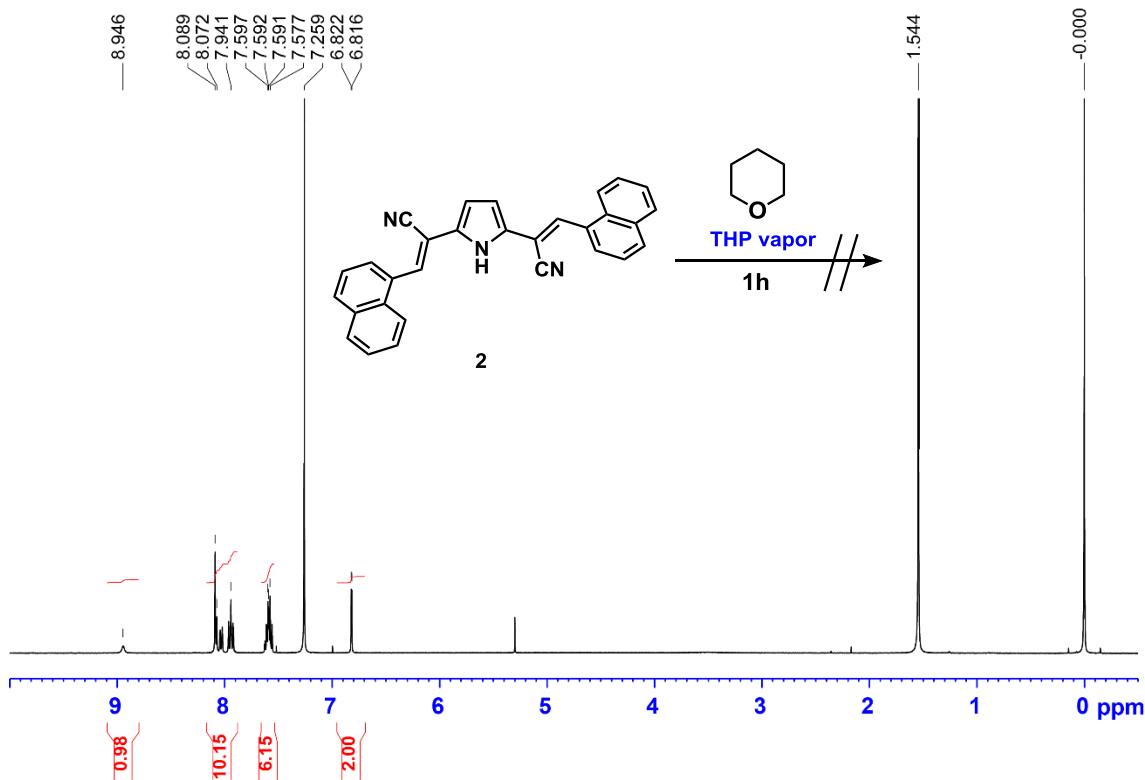


Figure S21 ¹H-NMR (400 MHz, CDCl₃) after exposing the pristine powder to tetrahydropyran (THP) vapor for 1h. Peaks of THP were not observed after the exposure.

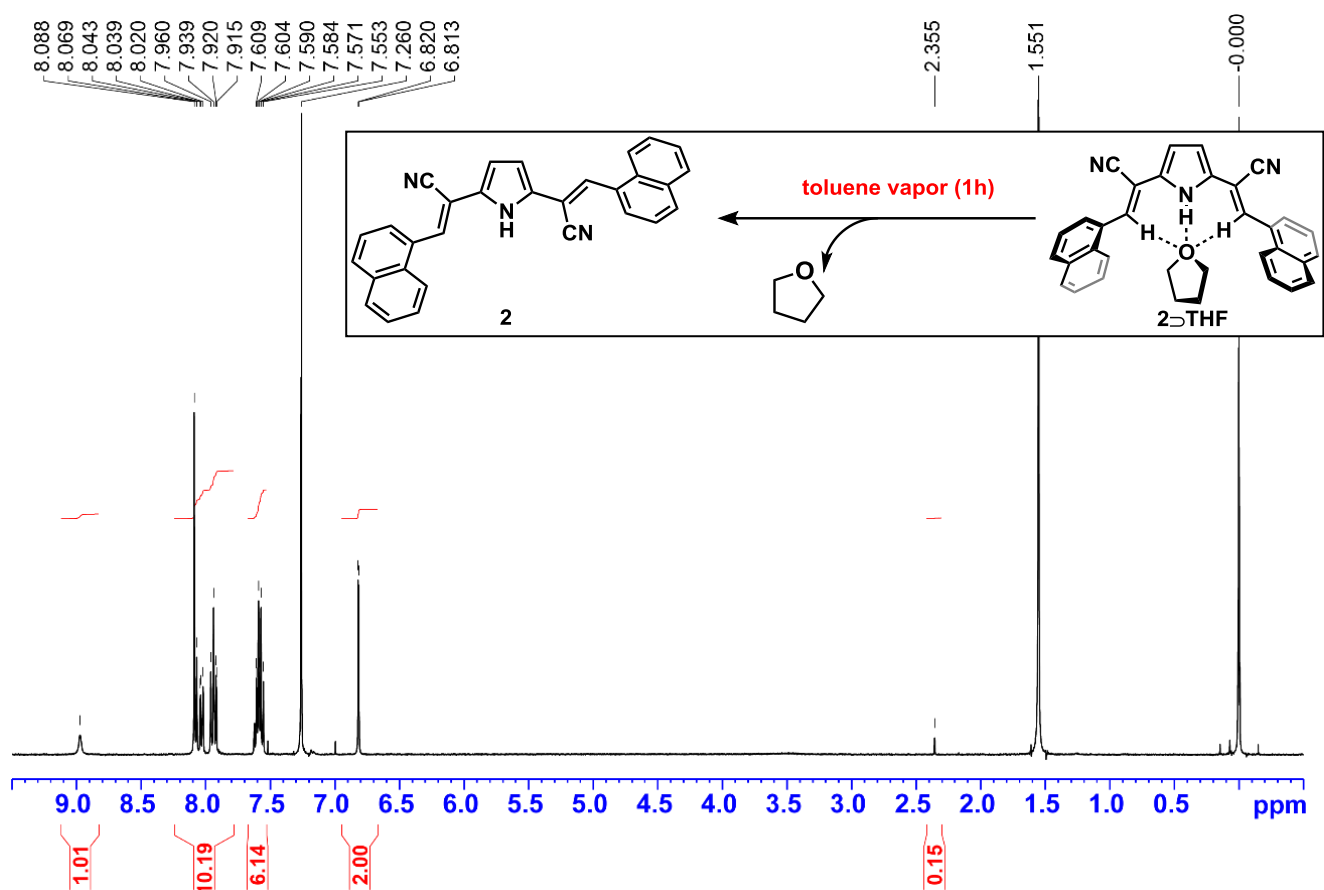


Figure S22 ¹H-NMR (400 MHz, CDCl₃) after exposure of **2·THF** powder to toluene vapor for 1h. The exposure of the **2·THF** powder to toluene for 1h.

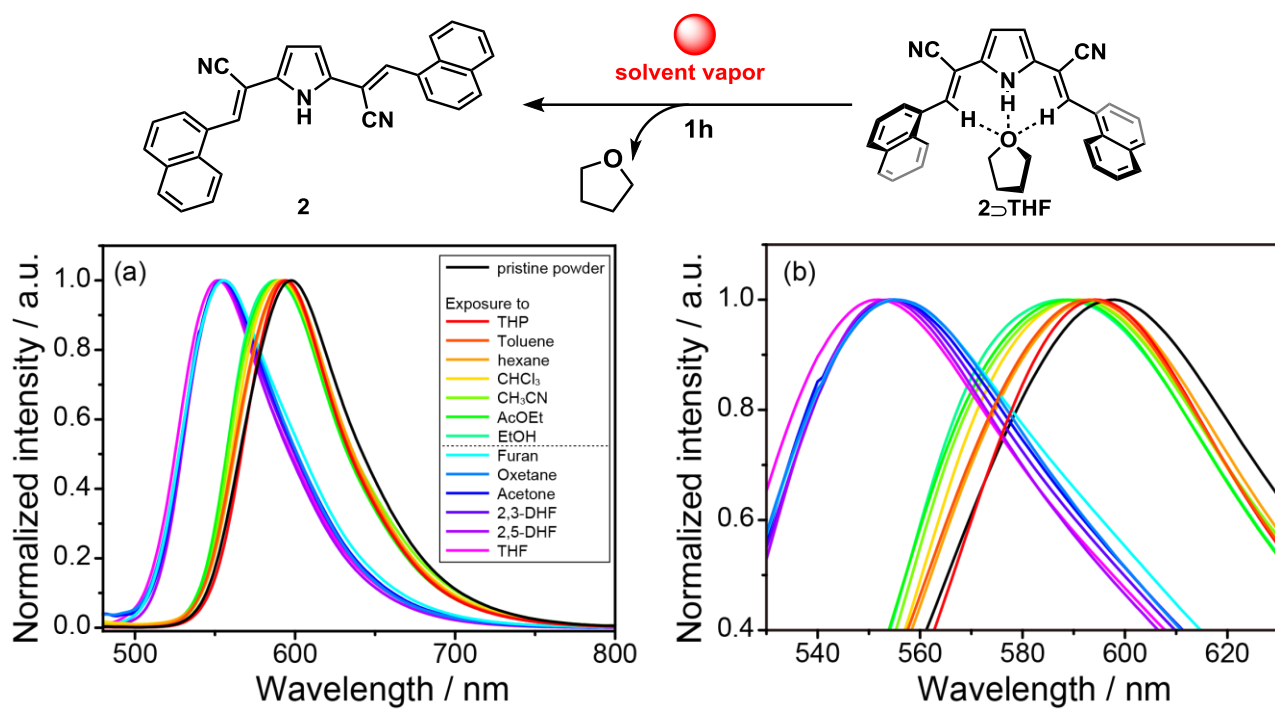


Figure S23 Fluorescence spectra after exposing **2·THF** powder to various solvent vapor for one hour. $\lambda_{\text{ex}} = 400$ nm. (b) An enlarged graph of (a).

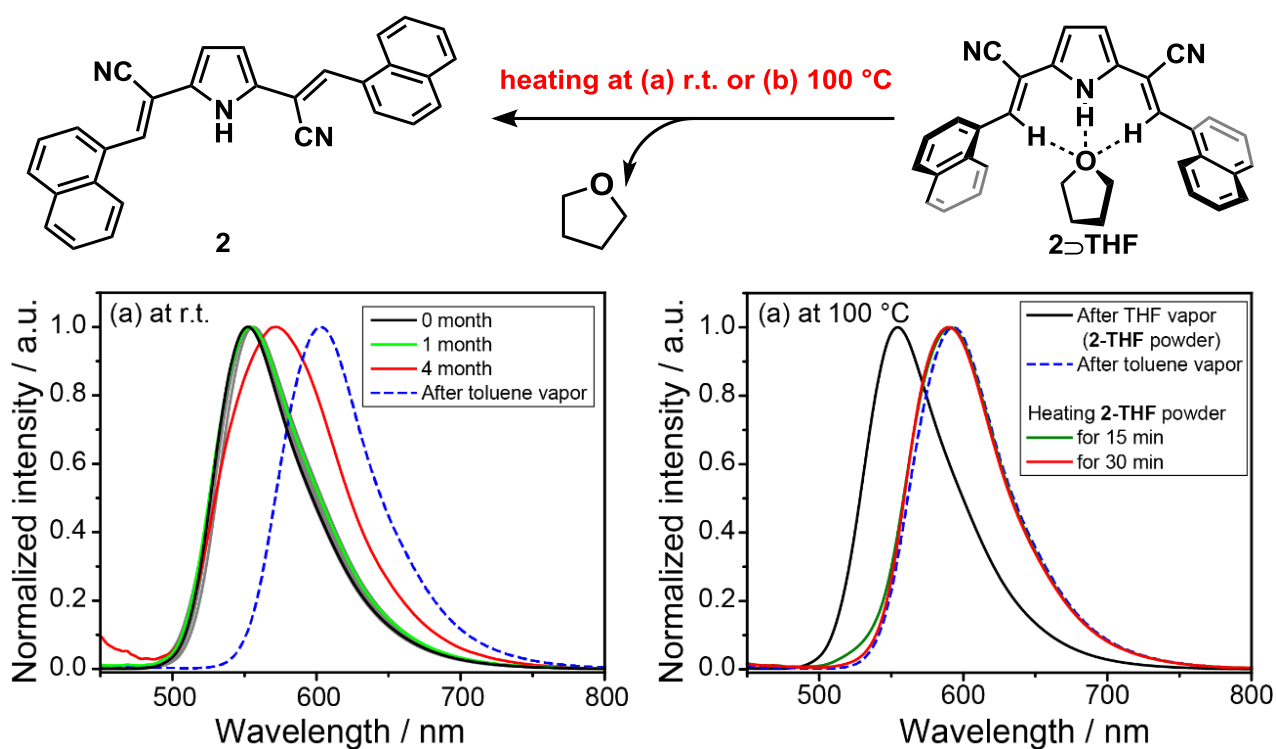


Figure S24 Thermal stability of **2**⊃THF powder (a) at r.t. and (b) at 100 °C.

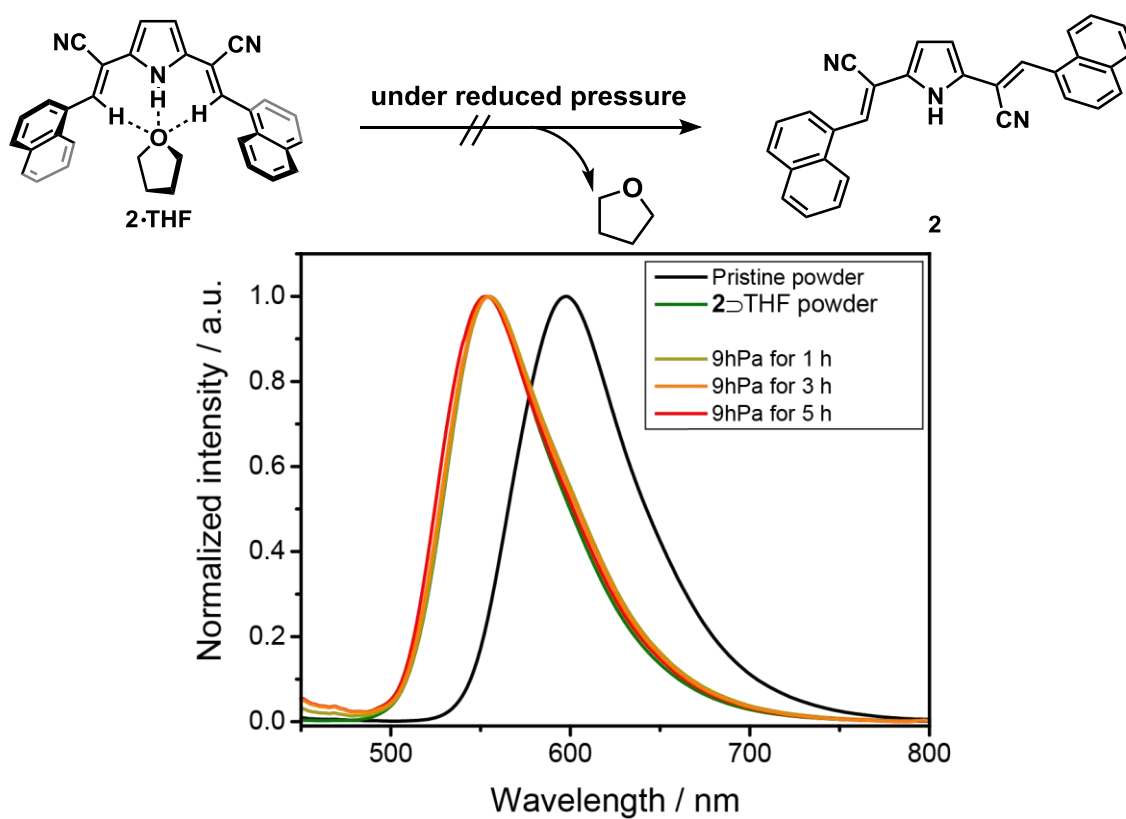


Figure S25 Fluorescence spectra change of the **2**⊃THF powder after drying under reduced pressure. The spectra were not almost changed for 5h.

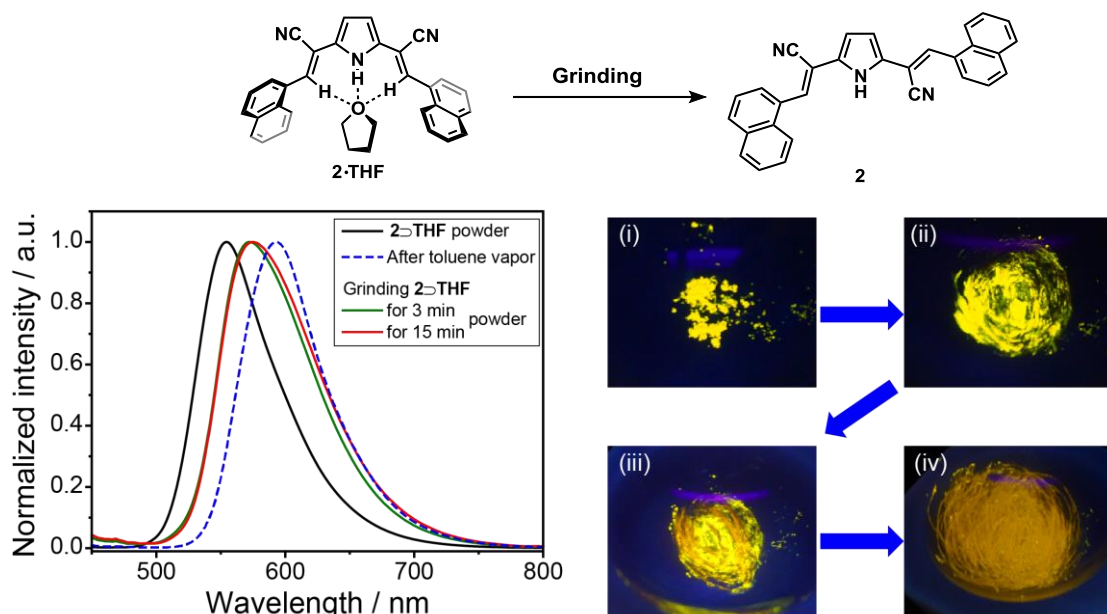


Figure S26 Fluorescence spectra change of the $2 \cdot \text{THF}$ powder by the grinding. The spectrum of the sample after grinding (red solid line) for 15 min was almost same as the spectrum for 3 min (green solid line).

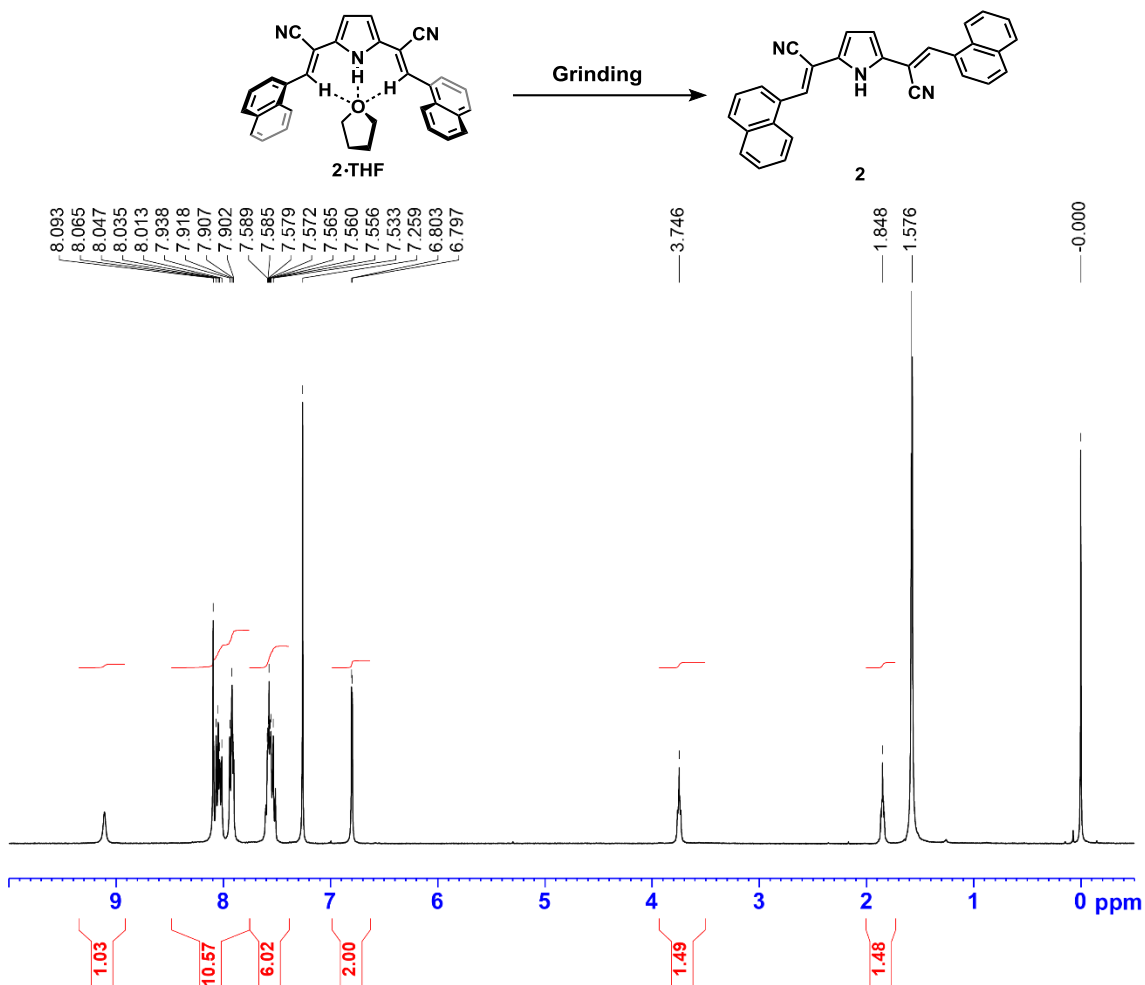


Figure S27 ^1H -NMR (400 MHz, CDCl_3) chart after grinding $2 \cdot \text{THF}$ powder for 15 min. The molar ratio of compound **2** and THF molecule became 2.7:1.

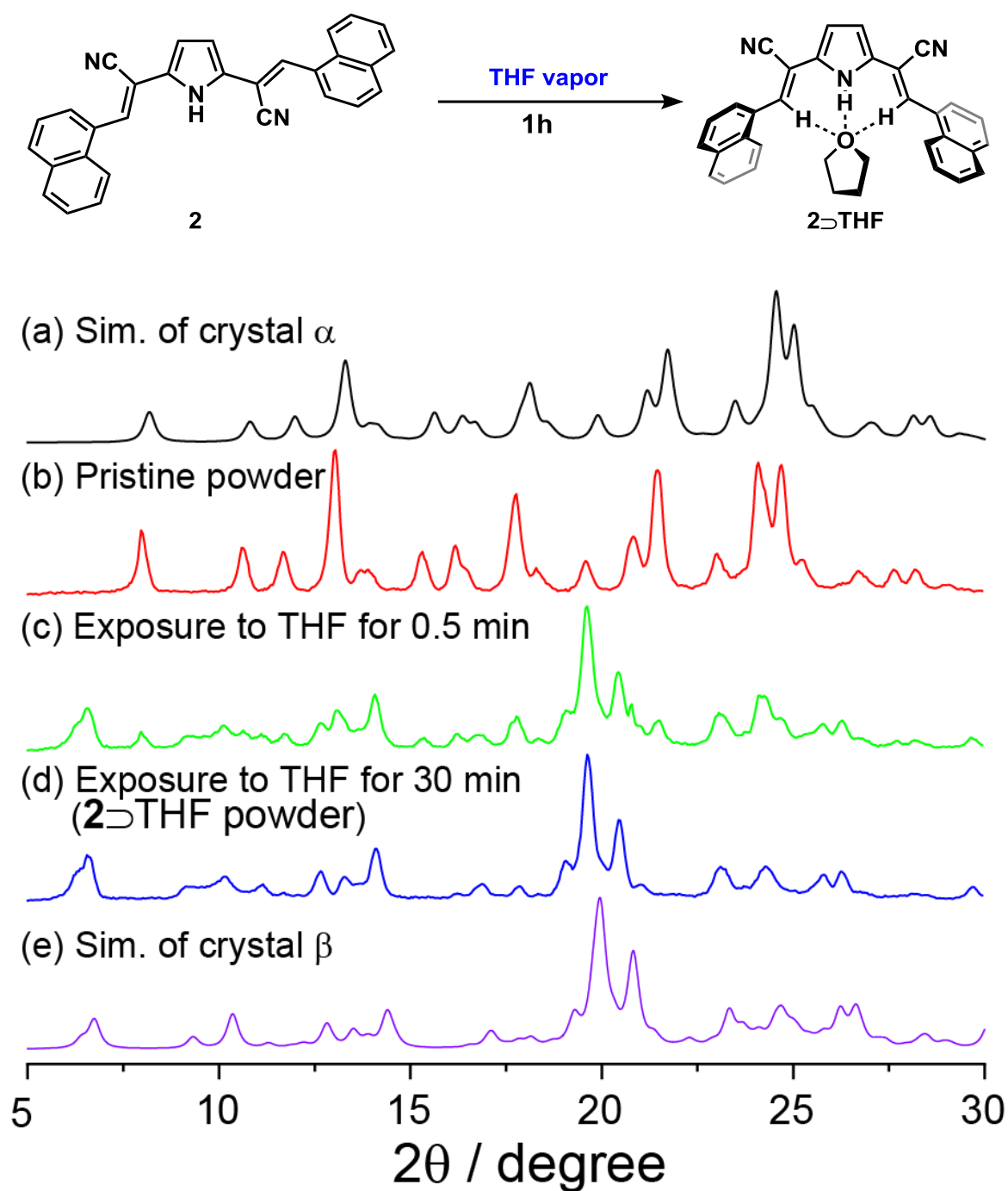


Figure S28 PXRD pattern changes of the pristine powder **2** upon the exposure to the THF vapor (forward process). The PXRD pattern of the crystal α and β was calculated from the X-ray single crystal data (FWHM = 0.35 °).

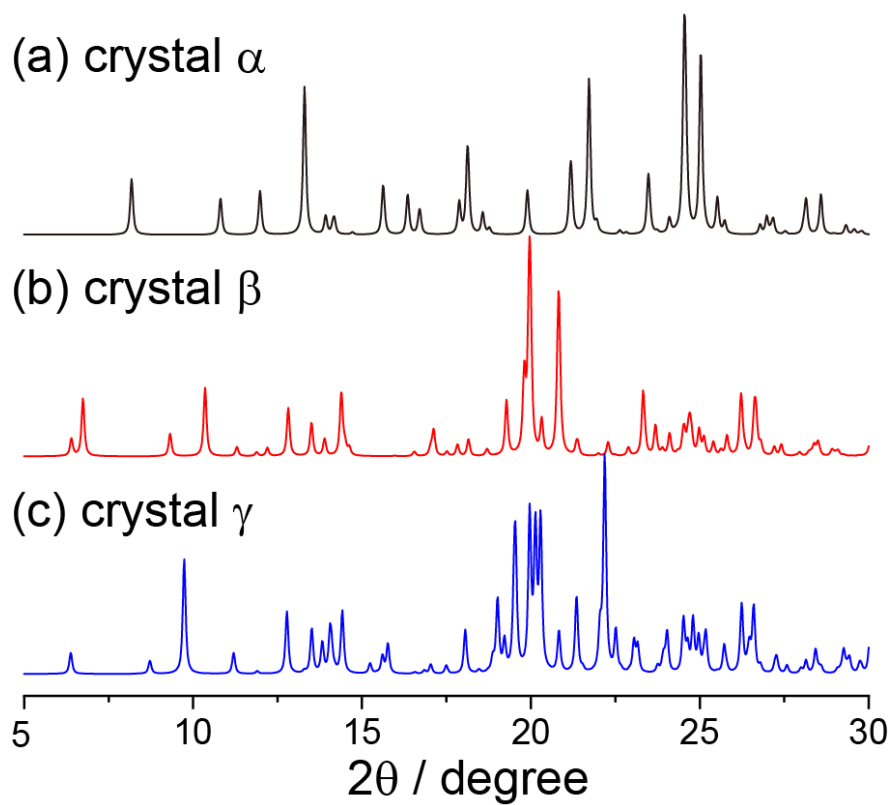


Figure S29 Simulated PXRD patterns of the crystal α and β obtained from the X-ray single crystal data (FWHM = 0.10 °).

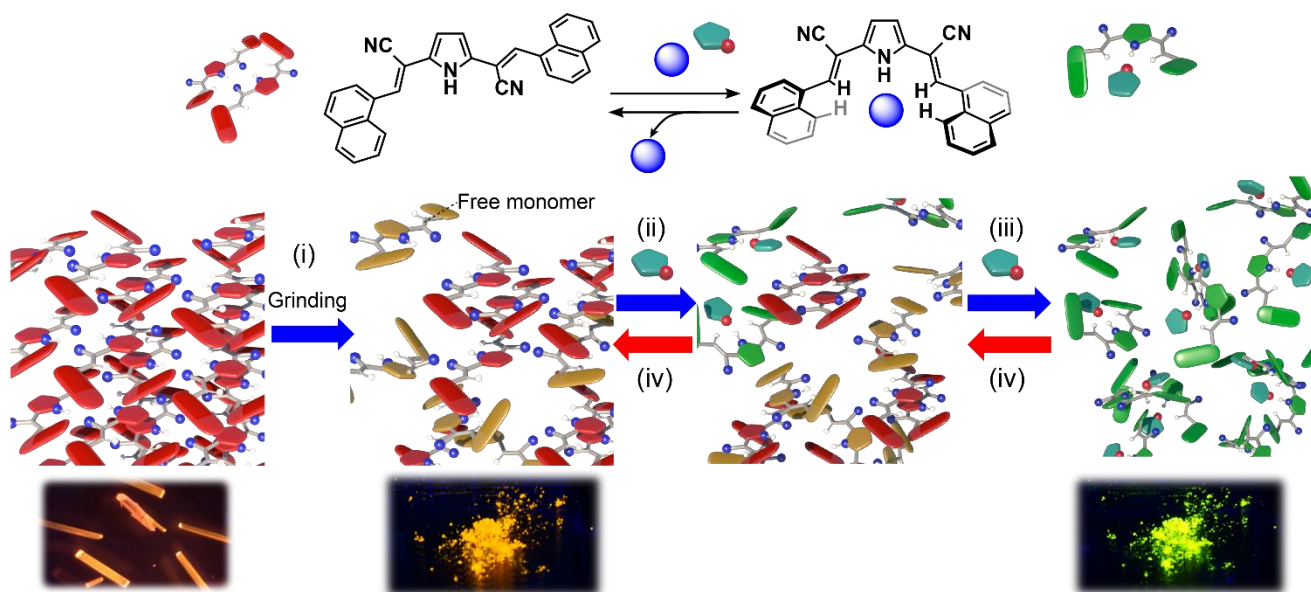
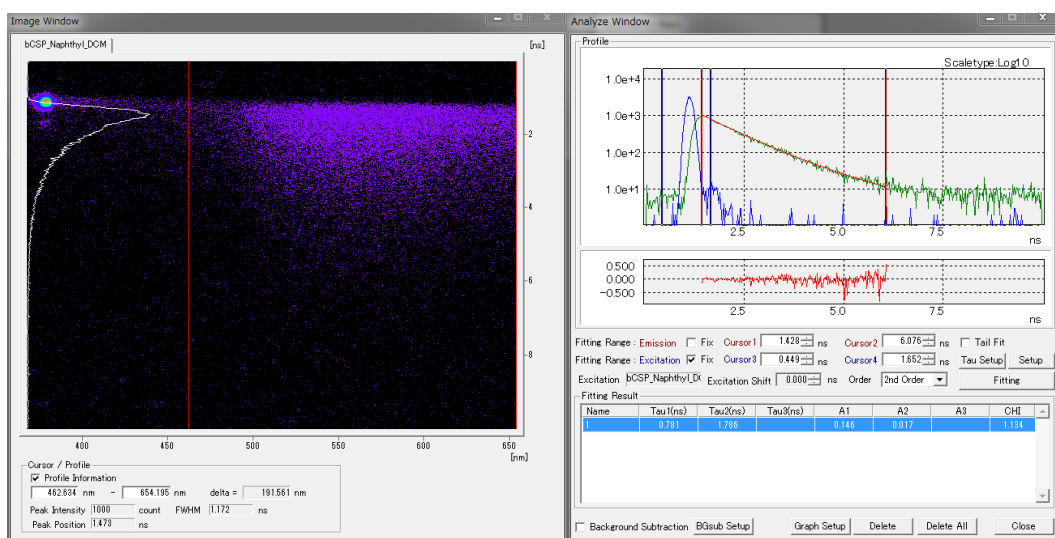
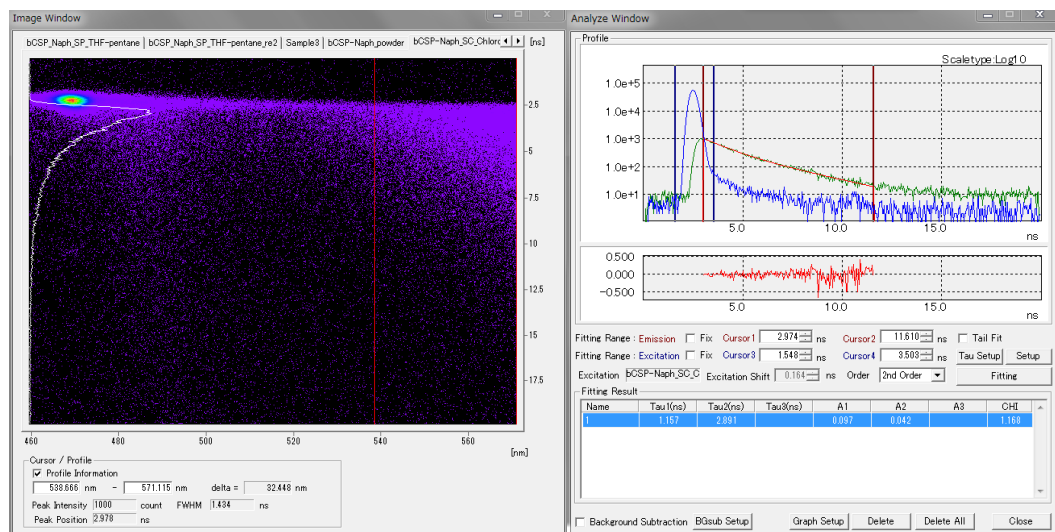


Figure S30 A plausible mechanism of vapochromism of the compound **2** in the powder state.

Table S5. Fluorescence lifetime of **2** in dichloromethane and at the single crystal state.^a

	τ_1 / ns	A_1	τ_2 / ns	A_2	χ	$\langle\tau_f\rangle$ / ns ^b
in DCM	0.781	0.146	1.786	0.017	1.134	0.99
single crystal α	1.16	0.097	2.891	0.042	1.168	2.06
single crystal β	2.95	0.038	4.027	0.071	1.247	3.72
single crystal γ	2.49	0.192	4.361	0.106	1.187	3.41

a. Fluorescence lifetimes were recorded upon excitation at 378 nm or 441 nm. *b.* The area-weighted ratio ($A_n\tau_n$) are shown in parentheses. *c.* The area-weighted mean fluorescence lifetime was calculated as follows: $\langle\tau_f\rangle = \Sigma(A_n\tau_n^2)/\Sigma(A_n\tau_n)$ where A_n is the coefficient of exponential function of the n -th component.

**Figure S31** (left) Streak image and (right) fluorescence decay analysis of **2** in DCM.**Figure S32** (left) Streak image and (right) fluorescence decay analysis of single crystal α in DCM.

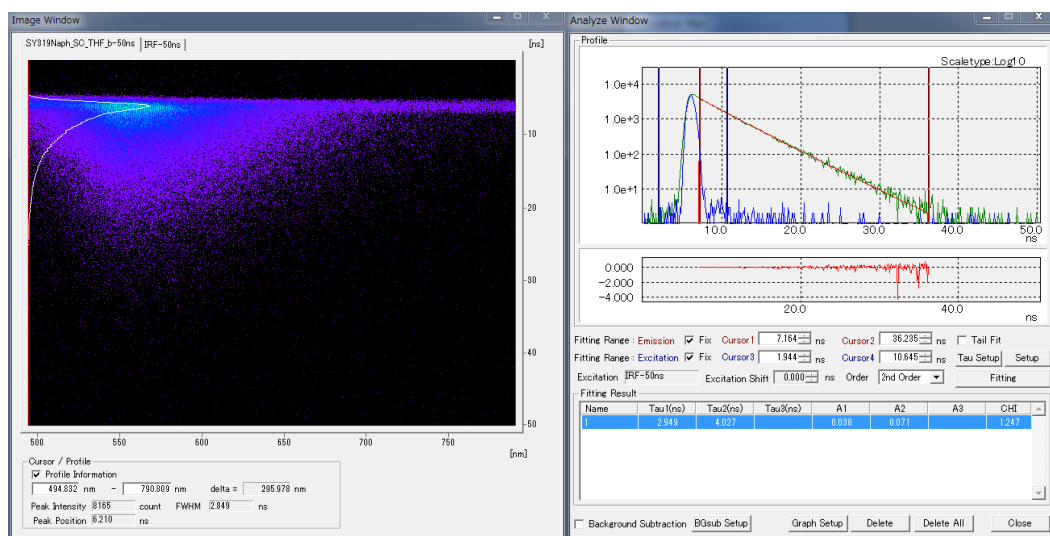


Figure S33 (left) Streak image and (right) fluorescence decay analysis of single crystal β in DCM.

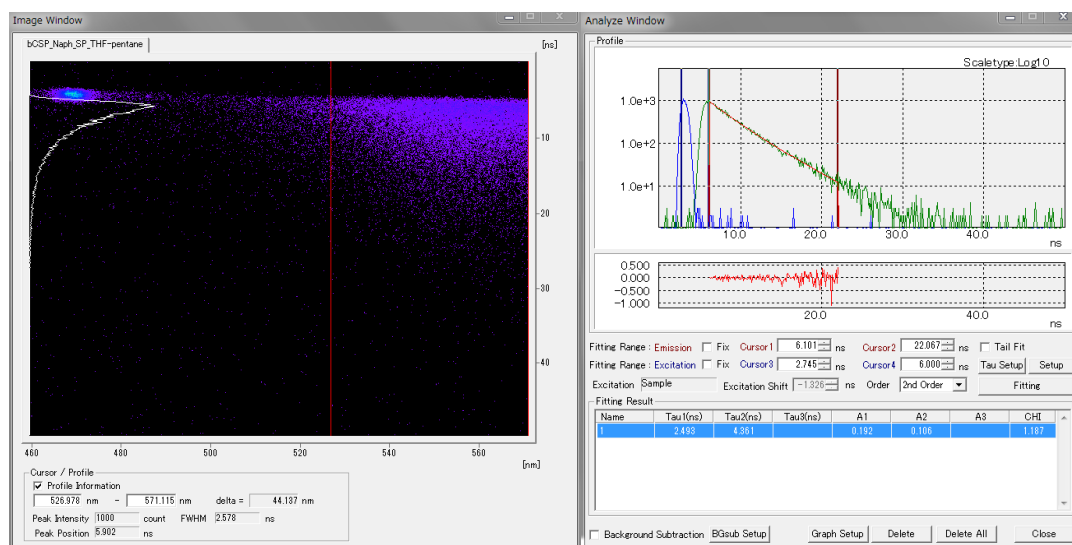


Figure S34 (left) Streak image and (right) fluorescence decay analysis of single crystal γ in DCM.

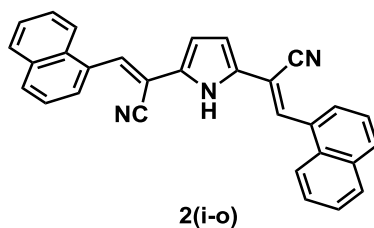


Table S6. Calculated excited states of the optimized structure **2(i-o)** at the TD-B3LYP/6-31g+(d,p) level on Gaussian 9 at the ground state (S_0).

No.	Energy (cm ⁻¹)	Wavelength (nm)	Osc. Strength	Major contribs	Minor contribs
1	20400	489.4	1.083	HOMO->LUMO (99%)	
2	24400	410.3	0.1057	H-1->LUMO (23%), HOMO->L+1 (75%)	
3	26200	382.0	0.0933	H-1->LUMO (74%), HOMO->L+1 (23%)	
4	28300	353.6	0.0044	H-2->LUMO (78%), HOMO->L+2 (15%)	H-1->L+1 (3%)
5	30100	332.2	0.0727	H-1->L+1 (78%)	H-2->LUMO (9%), HOMO->L+2 (7%), HOMO->L+3 (3%)
6	30600	326.4	0.0012	HOMO->L+2 (64%), HOMO->L+3 (17%)	H-2->LUMO (6%), H-1->L+1 (5%)
7	30800	325.1	0.0085	H-3->LUMO (78%)	H-3->L+1 (8%), H-1->L+5 (3%), HOMO->L+5 (9%)
8	31000	322.4	0.0066	H-4->LUMO (70%), HOMO->L+4 (17%)	H-4->L+1 (5%), H-1->L+4 (4%), HOMO->L+2 (2%)
9	31500	318.0	0.003	H-1->L+1 (10%), HOMO->L+3 (68%)	H-2->LUMO (2%), H-2->L+1 (4%), HOMO->L+2 (9%)
10	33300	299.9	0.0044	H-5->LUMO (19%), H-2->L+1 (74%)	HOMO->L+3 (3%)

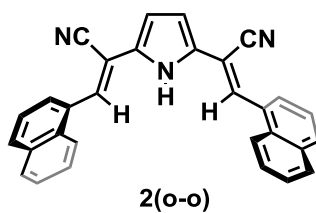


Table S7. Calculated excited states of the optimized structure **2(o-o)** at the TD-B3LYP/6-31g+(d,p) level on Gaussian 9 at the ground state (S_0).

No.	Energy (cm ⁻¹)	Wavelength (nm)	Osc. Strength	Major contribs	Minor contribs
1	20500	488.8	0.805	HOMO->LUMO (99%)	
2	24500	407.4	0.0046	H-1->LUMO (46%), HOMO->L+1 (52%)	
3	26500	377.9	0.3727	H-1->LUMO (51%), HOMO->L+1 (45%)	
4	28300	353.2	0.0181	H-2->LUMO (83%), HOMO->L+2 (14%)	
5	30400	328.6	0.0408	H-1->L+1 (68%), HOMO->L+2 (23%)	H-2->LUMO (8%)
6	30800	324.9	0.0024	H-3->LUMO (76%), HOMO->L+4 (10%)	H-4->L+1 (5%), H-1->L+5 (3%), HOMO->L+3 (5%)
7	30800	324.8	0.0119	H-4->LUMO (78%), HOMO->L+5 (10%)	H-3->L+1 (5%), H-1->L+4 (3%)
8	31100	321.9	0.0092	HOMO->L+3 (83%)	H-6->LUMO (3%), H-3->LUMO (5%), H-2->L+1 (4%)
9	31300	319.4	0.0025	H-1->L+1 (28%), HOMO->L+2 (59%)	H-2->LUMO (7%)
10	33300	300.1	0.0031	H-5->LUMO (63%), H-2->L+1 (33%)	

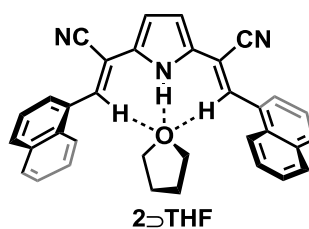


Table S8. Calculated excited states of the optimized structure **2(i-o)** at the TD-B3LYP/6-31g+(d,p) level on Gaussian 9 at the ground state (S_0).

No.	Energy (cm ⁻¹)	Wavelength (nm)	Osc. Strength	Major contribs	Minor contribs
1	20400	489.6	0.761	HOMO->LUMO (99%)	
2	24600	406.7	0.0493	H-1->LUMO (18%), HOMO->L+1 (80%)	
3	27000	369.9	0.278	H-1->LUMO (79%), HOMO->L+1 (18%)	
4	28500	350.5	0.0014	H-2->LUMO (54%), HOMO->L+2 (43%)	
5	30300	329.7	0.0342	H-2->LUMO (43%), HOMO->L+2 (50%)	H-1->L+1 (5%)
6	31000	322.4	0.0209	HOMO->L+3 (87%)	H-6->LUMO (4%), H-5->LUMO (3%), H-2->L+1 (3%)
7	31500	318.0	0.0071	H-4->LUMO (35%), H-1->L+1 (30%), HOMO->L+4 (25%)	H-3->L+1 (4%), H-1->L+5 (3%)
8	31500	317.7	0.0013	H-3->LUMO (49%), HOMO->L+5 (36%)	H-4->L+1 (6%), H-1->L+4 (4%)
9	31500	317.2	0.007	H-4->LUMO (15%), H-1->L+1 (62%), HOMO->L+4 (12%)	H-3->L+1 (2%), HOMO->L+2 (5%)
10	32600	306.7	0.0164	H-5->LUMO (92%)	H-2->L+1 (4%)

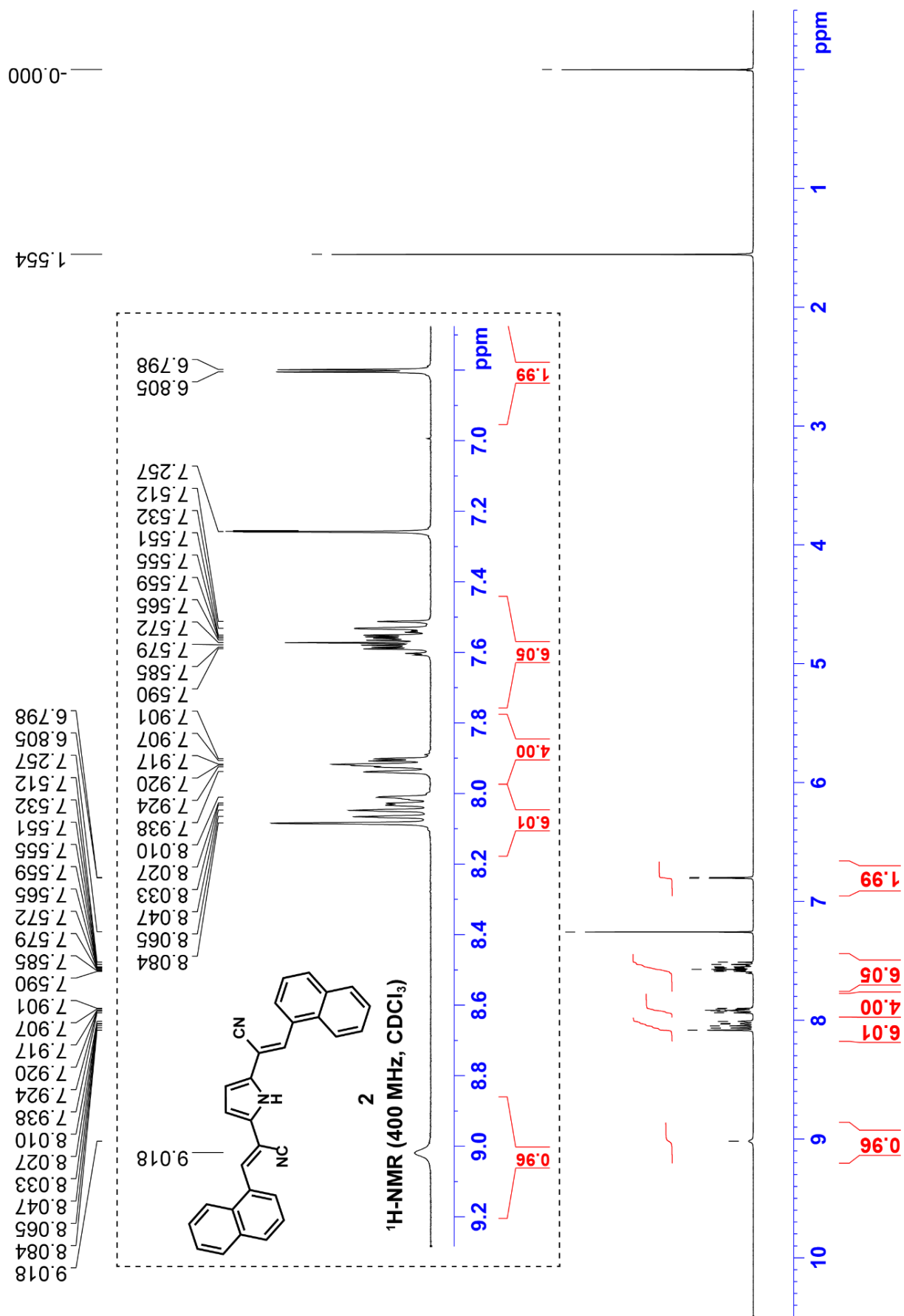


Figure S35 ¹H NMR (400 MHz, CDCl₃) chart of **2**.

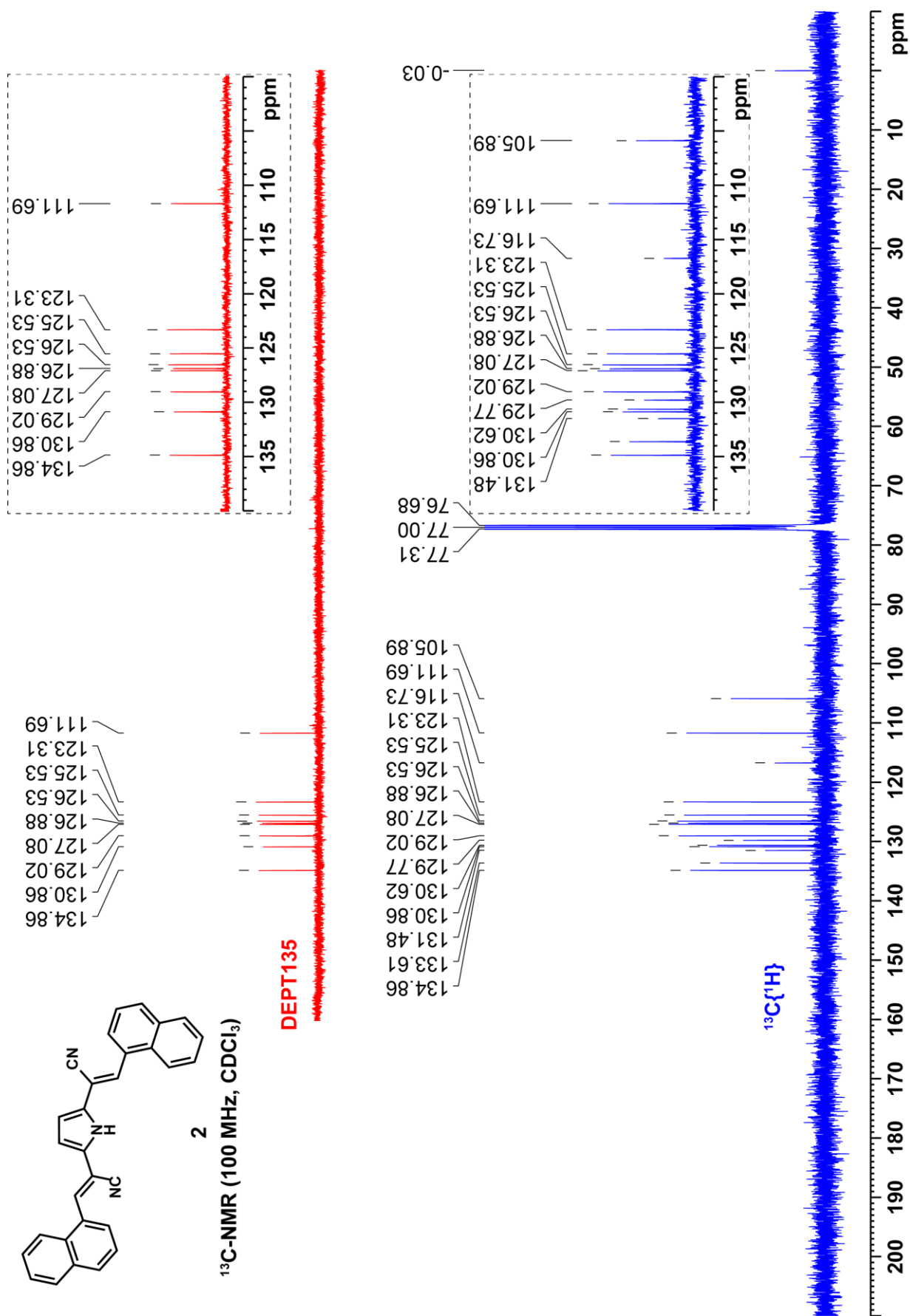
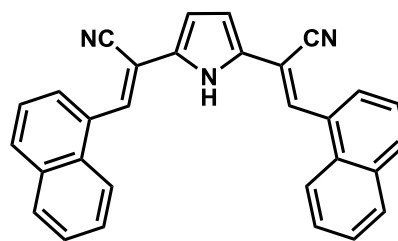


Figure S36 ¹³C NMR (400 MHz, CDCl₃) chart of **2**.

Cartesian coordinates [Å] of optimized structure of compound 2(o-o) at the ground state (S₀)

C	1.116126	2.415913	-0.191362	N	-4.180023	3.680206	1.114159
C	0.693779	3.743347	-0.125138	C	3.429029	2.849134	-0.798147
C	-0.693782	3.743348	0.125146	N	4.180027	3.680182	-1.114183
C	-1.116130	2.415915	0.191370	H	1.335439	4.605592	-0.235513
N	-0.000002	1.626835	0.000007	H	-1.335441	4.605594	0.235519
C	2.455116	1.874095	-0.385874	H	-0.000003	0.619715	0.000011
C	2.795426	0.568826	-0.163570	H	2.019250	-0.057117	0.269821
C	-2.455121	1.874098	0.385883	H	-2.019254	-0.057112	-0.269814
C	-2.795431	0.568828	0.163578	H	-4.518234	0.999515	2.202303
C	-4.065402	-0.107764	0.421176	H	-6.615563	-0.191595	2.694929
C	4.065399	-0.107762	-0.421171				
C	-4.845067	0.216948	1.527339				
C	-6.038312	-0.475233	1.820382				
C	-6.454445	-1.513747	1.016867				
C	-5.698642	-1.892865	-0.125231				
C	-4.493342	-1.182000	-0.444616				
C	4.493342	-1.182001	0.444615				
C	5.698646	-1.892860	0.125227				
C	6.454448	-1.513731	-1.016867				
C	6.038314	-0.475212	-1.820375				
C	4.845066	0.216962	-1.527329				
C	-6.123723	-2.958499	-0.965521				
C	-5.404212	-3.311671	-2.085689				
C	-4.228807	-2.597980	-2.417976				
C	-3.790966	-1.558270	-1.622673				
C	3.790965	-1.558281	1.622668				
C	4.228809	-2.597995	2.417965				
C	5.404217	-3.311680	2.085676				
C	6.123729	-2.958497	0.965511				
C	-3.429033	2.849138	0.798156				



2(o-o)

B3LYP/6-31g+(d,p)

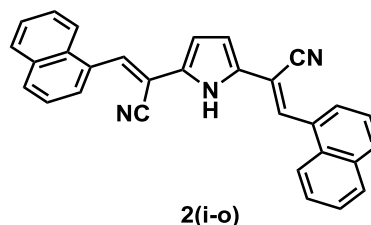
Int = Ultrafine

E(B3LYP) = -1318.93277788 hartree

of imaginary frequencies = 0

Cartesian coordinates [Å] of optimized structure of compound 2(i-o) at the ground state (S₀)

C	1.140061	1.800590	-0.034796	C	-1.722103	-1.022385	-1.057696
C	0.337160	2.899221	0.278822	N	-1.271648	-2.021302	-1.453900
C	-1.009326	2.504799	0.147441	C	3.280811	2.934143	0.138784
C	-1.023401	1.166575	-0.247202	N	3.782402	3.971596	0.302771
N	0.292730	0.762830	-0.350087	H	0.703434	3.873472	0.569130
C	2.593424	1.683031	-0.038535	H	-1.876545	3.129218	0.306046
C	3.269148	0.500826	-0.155039	H	0.573683	-0.149058	-0.681877
C	-2.127115	0.251817	-0.529977	H	2.657500	-0.397697	-0.164437
C	-3.434610	0.553836	-0.275500	H	-3.599912	1.503115	0.225657
C	-4.630774	-0.220739	-0.592955	H	-3.865140	-1.021088	-2.431594
C	4.709192	0.273312	-0.265865	H	-5.902459	-2.273655	-3.012519
C	-4.709377	-0.987561	-1.752399				
C	-5.881848	-1.691049	-2.096729				
C	-6.996234	-1.620352	-1.289949				
C	-6.978363	-0.849771	-0.096157				
C	-5.784651	-0.143735	0.273380				
C	5.291479	-0.921414	0.300181				
C	6.692510	-1.168385	0.109402				
C	7.478201	-0.229367	-0.611834				
C	6.906626	0.910674	-1.132195				
C	5.527538	1.154493	-0.966175				
C	-8.122175	-0.775247	0.745632				
C	-8.099094	-0.045218	1.913340				
C	-6.917738	0.634644	2.292373				
C	-5.790779	0.580228	1.497402				
C	4.547848	-1.862021	1.065006				
C	5.141057	-2.996508	1.580654				
C	6.517670	-3.246616	1.371490				
C	7.274265	-2.345610	0.655345				



B3LYP/6-31g+(d,p)

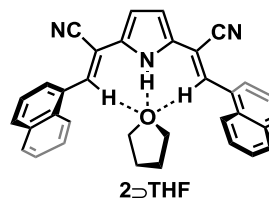
Int = Ultrafine

E(B3LYP) = -1318.93551959 hartree

of imaginary frequencies = 0

Cartesian coordinates [Å] of optimized structure of compound 2 \rightarrow THF at the ground state (S₀)

O	0.000190	-1.023312	-0.000476	H	4.544188	1.424181	2.216403
C	-0.330095	-1.854785	-1.142736	C	0.693183	4.096241	0.121532
H	0.192718	-1.455420	-2.017032	H	1.336085	4.957723	0.230708
H	-1.411134	-1.791616	-1.319385				
C	0.100518	-3.272810	-0.762575				
H	1.156074	-3.432092	-1.008452				
H	-0.490658	-4.036213	-1.275760				
C	0.330282	-1.855055	1.141602				
H	-0.191439	-1.454903	2.016190				
H	1.411526	-1.793303	1.317548				
C	-0.102354	-3.272531	0.761816				
H	-1.158132	-3.430246	1.007754				
H	0.487760	-4.036663	1.275145				
N	0.000142	1.970614	-0.000009				
H	0.000199	0.951868	-0.000162				
N	4.180538	4.082050	1.035806				
N	-4.180421	4.081763	-1.035783				
C	-4.111881	0.301799	-0.440860				
C	1.112167	2.765851	0.186589				
C	2.459746	2.242774	0.378921				
C	4.568682	-0.759224	-0.425776				
C	5.793704	-1.438313	-0.112305				
C	-1.111899	2.765757	-0.186997				
C	4.112188	0.301983	0.440816				
C	3.429483	3.239963	0.750409				
C	2.817680	0.937994	0.188074				
H	2.039303	0.282486	-0.192290				
C	-2.817281	0.937756	-0.188281				
H	-2.038855	0.282243	0.191985				
C	-2.459444	2.242552	-0.379162				
C	-4.568644	-0.758920	0.426149				
C	-3.429326	3.239673	-0.750507				
C	-0.692952	4.096178	-0.122357				
H	-1.335890	4.957611	-0.231705				
C	-3.873711	-1.147082	1.605250				
H	-2.975147	-0.613770	1.896022				
C	4.888519	0.648355	1.542129				



B3LYP/6-31g+(d,p)

Int = Ultrafine

E(B3LYP) = -1551.41674004 hartree

of imaginary frequencies = 0

References

- 1 C. Mazet, L. H. Gade, *Chem. Eur. J.* **2003**, 9, 1759–1767.
- 2 O. V. Dolomanov, L. J. Bourhis, R. J. Gildea, J. A. K. Howard, H. Puschmann, *J. Appl. Crystallogr.* **2009**, 42, 339.
- 3 G. M. Sheldrick, *Acta Crystallogr. Sect. A Found. Crystallogr.* **2015**, 71, 3.
- 4 G. M. Sheldrick, *Acta Crystallogr. Sect. C Struct. Chem.* **2015**, 71, 3.
- 5 Gaussian 09, Revision C.01, M. J. Frisch, G. W. Trucks, H. B. Schlegel, G. E. Scuseria, M. A. Robb, J. R. Cheeseman, G. Scalmani, V. Barone, B. Mennucci, G. A. Petersson, H. Nakatsuji, M. Caricato, X. Li, H. P. Hratchian, A. F. Izmaylov, J. Bloino, G. Zheng, J. L. Sonnenberg, M. Hada, M. Ehara, K. Toyota, R. Fukuda, J. Hasegawa, M. Ishida, T. Nakajima, Y. Honda, O. Kitao, H. Nakai, T. Vreven, J. A. Montgomery, Jr., J. E. Peralta, F. Ogliaro, M. Bearpark, J. J. Heyd, E. Brothers, K. N. Kudin, V. N. Staroverov, T. Keith, R. Kobayashi, J. Normand, K. Raghavachari, A. Rendell, J. C. Burant, S. S. Iyengar, J. Tomasi, M. Cossi, N. Rega, J. M. Millam, M. Klene, J. E. Knox, J. B. Cross, V. Bakken, C. Adamo, J. Jaramillo, R. Gomperts, R. E. Stratmann, O. Yazyev, A. J. Austin, R. Cammi, C. Pomelli, J. W. Ochterski, R. L. Martin, K. Morokuma, V. G. Zakrzewski, G. A. Voth, P. Salvador, J. J. Dannenberg, S. Dapprich, A. D. Daniels, O. Farkas, J. B. Foresman, J. V. Ortiz, J. Cioslowski, and D. J. Fox, Gaussian, Inc., Wallingford CT, **2010**.
- 6 N. M. O'Boyle, A. L. Tenderholt and K. M. Langner. *J. Comp. Chem.* **2008**, 29, 839-845.
- 7 N. J. Turro, V. Ramamurthy, J. C. Scaiano, *Principles of Molecular Photochemistry: An Introduction*; University Science Books:Sausalito, CA, **2009**.